Seasonal variability, sources, and parameterization of ice-nucleating particles in the Rocky Mountain region: Importance of soil dust and biological contributions

Ruichen Zhou, Russell Perkins, Drew Juergensen, Kevin Barry, Kelton Ayars, Oren Dutton, Paul DeMott, Sonia Kreidenweis

Department of Atmospheric Science, Colorado State University, Fort Collins, Colorado 80523, USA

Corresponding author: Russell Perkins (rperkins@colostate.edu)

Abstract

13   Atmospheric ice-nucleating particles (INPs) significantly influence cloud microphysics and

14   aerosol-cloud interactions. Understanding INPs in mountain regions is important for predicting

15   impacts on regional clouds and precipitation. In this study, we conducted comprehensive

16   measurements of immersion-freezing INPs at Mt. Crested Butte in the Rocky Mountains from

17   September 2021 to June 2023 as part of the Surface Atmosphere Integrated Field Laboratory (SAIL)

18   campaign. The average number concentration of INPs active at −20 °C was 2 L^{-1}, with distinct

19   seasonal variation characterized by high summer concentrations and low winter concentrations.

20   Aerosol sources were resolved, and INP concentrations were correlated with a coarse dust aerosol

21   type, which dominates PM_{10} in this region. Calculating IN active surface site densities (n_s) further

22   supporting the primary contribution from coarse dust to INPs. Treatment with H_2O_2 indicated

23   substantial contributions (91% on average) from organic INPs across all activation temperatures,

24   suggesting that supermicron organic-containing soil dust dominates the INPs in this region. Heat-

25   labile INPs, likely biological in origin, were identified as dominant at > −15 °C through heat

26   treatment of samples and showed significantly lower contributions in winter (~96% reduction).

27   Parameterizations based on n_s for the INPs observed in this mountainous region were developed,

28   which effectively reproduced measured INP concentrations, particularly when accounting for

29   seasonal differences. This study provides the first long-term, comprehensive characterization of

30   INPs for the Upper Colorado River Basin region and offers a parameterization potentially useful

31   for predicting INPs in other remote continental regions.

1. Introduction

Atmospheric aerosols play critical roles in forming clouds, and inadequate understanding of aerosol-cloud interactions presents one of the largest uncertainties in predicting global climate (IPCC, 2022; Seinfeld et al., 2016). The subset of aerosol particles that serves as ice-nucleating particles (INPs) can trigger heterogeneous freezing of cloud water droplets, allowing them to freeze above the homogeneous freezing temperature (approximately $-38°C$) (Hoose and Möhler, 2012). Among the mechanisms of heterogeneous freezing, this immersion freezing process is considered the most important process for mixed-phase clouds, which are common at midlatitudes in all seasons (Kanji et al., 2017; De Boer et al., 2011). These INPs are responsible for a significant proportion of initial cloud ice phase formation, thus impacting the Earth's radiative balance and precipitation (Lohmann and Feichter, 2005; Kanji et al., 2017; Burrows et al., 2022). Although INPs are increasingly a focus of study, the sources and abundances of INPs are not well characterized for many regions.

Various aerosol sources have been found to contribute to INPs, including natural and anthropogenic sources (Kanji et al., 2017). Atmospheric mineral dust particles are considered a dominant contributor of INPs throughout much of the troposphere (Murray et al., 2012; Hoose and Möhler, 2012), and they produce high INP concentrations in a mass or surface area basis at temperatures lower than $-15°C$ (Atkinson et al., 2013; Kiselev et al., 2017). Mineral INPs are inorganic components that are lofted from rock or soil and can undergo long range transport to remote areas (Knippertz and Stuut, 2014). In contrast, soil dusts from agricultural or grazed fields (arable soils) were suggested to contribute 25% of the global dust burden (Ginoux et al., 2012), and were found to initiate ice nucleation at temperatures as high as $-6°C$ (Garcia et al., 2012; O'Sullivan et al., 2014). Organics in arable soil dust are suggested as the main contributors to their

55   ice nucleating ability (Tobo et al., 2014; Hill et al., 2016). Biomass burning aerosols and fly ash

56   also contribute to INP populations and have received increasing attention under global warming

57   and the accompanying more frequent and intense wildfires (Prenni et al., 2012; McCluskey et al.,

58   2014; Umo et al., 2015). Biomass burning aerosols typically present lower ice nucleating ability,

59   defined as the IN active surface site density for ice nucleation on particle surfaces (i.e., INP

60   concentration/aerosol surface area concentration), compared to dust particles, while atmospheric

61   aging can potentially enhance their ice nucleating ability (Jahl et al., 2021). Biogenic aerosols,

62   such as primary biological particles composed of bacteria, pollen, fungal spores, and their

63   fragments, were identified in the 1970s as important INP sources (Vali and Schnell, 2024; Schnell

64   and Vali, 2024). They typically can activate ice formation at a warmer temperature than other INPs

65   listed above and thus may control first ice formation in clouds (Pratt et al., 2009; Creamean et al.,

66   2013; Tobo et al., 2013). Besides these INP sources, marine aerosol (Wilson et al., 2015;

67   McCluskey et al., 2018b), secondary organic aerosol, and fuel-combustion aerosols can contribute

68   to INPs (Kanji et al., 2017).

69   To estimate INPs for use in numerical cloud models, early parameterizations were typically based

70   on empirical relationships between INPs and temperature or supersaturation alone (Bigg, 1953;

71   Meyers et al., 1992). These parameterizations could show large biases compared to field

72   observations. DeMott et al. (2010) proposed a widely used parameterization based on temperature

73   and number concentrations of particles larger than 0.5 µm in diameter, which has been applied in

74   global and regional models due to its convenience and independence from detailed aerosol

75   composition (Miltenberger et al., 2018; Storelvmo et al., 2011; Burrows et al., 2022). However,

76   recent studies highlight the need for more physically based and source-specific parameterizations

77   (Burrows et al., 2022; Shi and Liu, 2019; DeMott et al., 2015). Laboratory and field studies have

78   shown that different aerosol types (e.g., mineral dust, biological particles, marine aerosols) exhibit

79   distinct ice-nucleating efficiencies (Hoose and Möhler, 2012; Kanji et al., 2017). Parameterizations

80   based on the ice-nucleating IN active surface site density ($n_s(T)$) have been developed for various

81   aerosol types under immersion freezing conditions (Niemand et al., 2012; DeMott et al., 2015;

82   Harrison et al., 2019; McCluskey et al., 2018a; Umo et al., 2015; Schill et al., 2020; Tobo et al.,

83   2014; O'Sullivan et al., 2014). Further field observations and laboratory studies are needed to

84   improve these parameterizations and reduce uncertainties in INP predictions.

85   Mountainous regions, covering approximately one-quarter of the global land surface, play a critical

86   role in regional and global hydrological and climatic systems. Importantly, they are sources of

87   freshwater supporting nearly half of the world's population (Viviroli et al., 2007). Cloud and

88   precipitation formation in mountainous areas are strongly influenced by aerosol–cloud interactions

89   (Lynn et al., 2007). The presence, variability, and sources of INPs in mountain areas can

90   significantly affect cloud phase, lifetime, and precipitation efficiency (Creamean et al., 2013; Lynn

91   et al., 2007). However, INP observations in mountain environments, especially for long-term

92   continuous measurements, are limited (Lacher et al., 2018; Sun et al., 2024; Conen et al., 2015),

93   hampering our understanding of INP major sources, seasonal variation, and the influence of

94   complex mountain terrain on their vertical distribution. Improved understanding of INPs in

95   mountainous regions is essential for better representation of clouds and precipitation formation in

96   weather and climate models, and for predicting future changes in water availability under global

97   climate change regimes.

98   The Surface Atmosphere Integrated Field Laboratory (SAIL) Campaign, conducted from

99   September 2021 to June 2023 in the Upper Colorado River Basin of the Rocky Mountains,

100 included aims to improve understanding of how aerosols, particularly long-range transported dust

101 and wildfire smoke, affect the surface energy and water balance through their impacts on cloud,

102 precipitation, and surface albedo, and how these effects vary by season (Feldman et al., 2023).

103 This campaign provided a unique opportunity to investigate INPs in the Colorado Rocky

104 Mountains over a nearly two-year period. This study presents comprehensive measurements of

105 immersion-freezing INPs, including their seasonal and temperature-dependent variability, as well

106 as associations with aerosol sources. We further explore different INP compositional types,

107 biological/heat-labile, other organic, and inorganic INPs, and their inter-relationships, highlighting

108 the importance of organic INPs. A parametrization method is proposed for INPs in this region that

109 reproduces the observed two-year INP concentration record.

110

111 2. Methods

112 2.1 Sampling site and sample collection

113 The SAIL campaign deployed the Department of Energy Atmospheric Radiation Measurement

114 (DOE ARM) Mobile Facility 2 (AMF-2) at the East River Watershed, which is located near Crested

115 Butte and Gothic, Colorado (Feldman et al., 2023). This mountainous region, with elevations

116 ranging from ~2440 to 4350 m above sea level, is characterized by complex terrain, a deep seasonal

117 snowpack, and pronounced hydrometeorological gradients. The region experiences strong

118 seasonal contrasts, with cold snowy winter and warm summers influenced by convective activity

119 associated with the North American monsoon (Feldman et al., 2023).

120 For INP analyses, aerosol filter samples were collected by DOE ARM technicians through the INP

121 Mentor Program approximately every three days from September 2021 to June 2023, with each

122 sampling period lasting about 24 hours, as described in the instrument handbook (Creamean et al.,

123   2024) and repeated briefly here. Aerosols were collected on two 47 mm Nuclepore polycarbonate

124   filters (0.2 μm pore size) at flow rates in the range of 10–18 lpm, with total sampling volumes of

125   approximately 15000 to 25000 L. For computing atmospheric concentrations in this study, the

126   sampling volume was corrected to standard temperature (273.15 K) and pressure (101.3 kPa). Prior

127   to sampling, the filters were cleaned using 10% H_2O_2 and deionized (DI) water to remove organic

128   and biological residues, then stored in sterile Petri dishes. For the first month (September 2021) of

129   the campaign, samples were collected at the M1 site (38°57′22.35″N, 106°59′16.66″W at 2885 m

130   MSL). From October 2021 to June 2023, samples were collected at the S2 site (38°53′52.66″N,

131   106°56′35.21″W at 3137 m MSL). The distance between M1 and S2 sites is about 8 km. The

132   possible difference in INP concentrations at M1 in the first month is not addressed here, since this

133   study is aimed at representing the INPs in this region, and there was no significant change in INP

134   concentrations when moving from the M1 to the S2 site. All samples were stored at −20 °C after

135   collection, during shipment, and until the analysis in the laboratory.

136

2.2 Laboratory Ice Spectrometer analysis of filter-collected particles

138   The immersion freezing ability of particles collected on filters was quantified using the Colorado

139   State University (CSU) Ice Nucleation Spectrometer (INS), following established procedures

140   (McCluskey et al., 2017; Hiranuma et al., 2015; Barry et al., 2021a), which are the same methods

141   used by the DOE ARM INP Mentor Program (Creamean et al., 2024). The INP Mentor Program

142   analyzed many of the samples from the SAIL campaign. Our analysis was used to fill gaps in time

143   for the Mentor Program samples, and provide additional heat and hydrogen peroxide treatments,

144   described below. Our data on these samples is provided within the Mentor Program data product

145   (Shi et al., 2025). Briefly, exposed filters were mixed with 10 mL of filtered deionized water in a

146   centrifuge tube, then rotated for 20 minutes using an end-over-end shaker to resuspend the particles.

147   Aliquots of the resuspension solution were pipetted into a 96-well PCR tray and cooled at a rate

148   of 0.33 °C min^{-1} from room temperature to −30 °C in the CSU INS. The number of frozen wells

149   was recorded at 0.5 °C intervals. Cumulative INP concentrations as a function of temperature

150   ($n_{INPs}(T)$, INPs per liter of air) were calculated based on the method of Vali (1971) using:

151
$$n_{INPs}(T) = ln(\frac{N_0}{N_0 - N(T)}) \times \frac{V_w}{V_c} \times \frac{1}{V_a}$$

152   where N_0 is the total number of wells containing aliquots, $N(T)$ is the cumulative number of wells

153   frozen at temperature T, V_w is the volume of water used for particle resuspension, V_c is the aliquot

154   volume added to each well, and V_a is the total sampled air volume. Counting uncertainties were

155   estimated using binomial confidence intervals (Agresti and Coull, 1998). Field blank filters were

156   collected every month by briefly exposing them at the sampling site for several seconds before

157   storage. Before calculating INP concentrations, the average number of INPs versus temperature

158   per blank filters was subtracted from the calculated number of INPs versus temperature per sample

159   filter, to account for potential contamination during sampling and handling, as well as any residual

160   contamination on the filters after cleaning.

161   To further characterize the types of INPs, portions of the suspended aerosol solution were subjected

162   to heat and hydrogen peroxide (H_2O_2) treatments, followed by freezing analysis of aliquots of these

163   portions. For heat treatment, the solution was heated to 95 °C for 21 min before measurement. This

164   process inactivates the biological INPs by denaturation of proteins and removes heat-labile INPs

165   (O'Sullivan et al., 2014; Tobo et al., 2014; Hill et al., 2016). In total, 43 samples were exposed to

166   95 °C heat treatment, and their temperature spectra are shown in Figure S1. In the peroxide

167   treatment, 30% H_2O_2 was added to the solution to make a final concentration of 10%, and the

168 mixture was heated at 95 °C for 21 min under UVB light to digest organics (Suski et al., 2018),

169 and the INPs remaining were presumed to be inorganic. A total of 34 samples underwent H_2O_2

170 treatment, with their temperature spectra shown in Figure S2. By comparing untreated (base), heat-

171 treated, and H_2O_2-treated results, INPs were categorized into biological/heat-labile, other organic,

172 and inorganic types. Daily et al. (2022) found that some minerals also showed reduced immersion-

173 freezing activity after heat treatment; however, SAIL samples showed some difference with the

174 behaviors they reported. For minerals with initial active temperatures > −10 °C, IN active surface

175 site density either decreased at all measured temperatures (Arizona Test Dust (ATD) and Fluka

176 Quartz) or was not sensitive to wet heating (K-feldspar) (Daily et al., 2022), differing from some

177 spectra of SAIL samples that only showed decreases at warm temperatures and almost no change

178 at temperatures < −18 °C (Figure S1). This suggests that mineral INPs have limited contributions

179 to the decreases of INP concentrations after heat treatment in the SAIL samples.

180 There were eight ground-based sites within 55 km of the SAIL sampling locations conducted

181 orographic cloud seeding operations by North American Weather Consultants Inc., targeting

182 precipitation enhancement. To the best of our knowledge, these seeding stations combusted

183 solutions in a propane flame, producing particles containing silver iodide (AgI) and other inorganic

184 salts that served as seeding aerosols. These seeding activities occurred in specific storm situations

185 during winter and early spring and strongly impacted our INP observations. The measured

186 concentrations of INPs active at temperatures from −7.5 °C to −27.5 °C for a total of 113 24-hour

187 samples are shown in Figure S3. Since this work focuses on investigating the natural or background

188 INPs in the Rocky Mountain region, samples collected on days that overlapped with artificial cloud

189 seeding activities, as recorded in their logbook (data provided by North American Weather

190 Consultants Inc.), are highlighted in Figure S3 and excluded from the discussion below. Cloud

191 seeding activities last less than 24 hours, typically 4-8 hours, and are unlikely to affect the

192 subsequent sample collected 3 days later. Also, eight samples collected during winter exhibited

193 distinct INPs spectra from other samples, but highly similar to the INP spectrum of Snomax®, a

194 commercial non-living bacterial INP product used in snowmaking (Figure S4a). Furthermore, *P.*

195 *syringae,* the bacterium type in Snomax, was identified in some of these samples based on qPCR

196 analysis (Supplement Text S2, Figure S4b). These samples are highly suspected to have been

197 affected by snowmaking activities during wintertime, associated with the location of sampling site

198 within a ski resort at Crested Butte. Therefore, these samples, along with those affected by cloud

199 seeding activities, were excluded from the subsequent discussion to better understand the

200 characteristics of natural INPs in the Rocky Mountain region.

201

202 **2.3 Source apportionment**

203 To investigate aerosol sources in the SAIL region, source apportionment was performed using

204 positive matrix factorization (PMF). PMF is a receptor model that decomposes an observation

205 matrix into factor profiles and their corresponding contributions related to emission sources and/or

206 atmospheric processes, providing a quantitative assessment of source influences (Paatero and

207 Tapper, 1994). Data from the Interagency Monitoring of Protected Visual Environments

208 (IMPROVE) site at White River, located approximately 30 km north of the SAIL campaign site,

209 were used for PMF analysis. The IMPROVE network (Malm et al., 1994) has collected 24-hour

210 aerosol filter samples every three days over several decades at this site, providing a valuable dataset

211 to understand aerosol sources and their long-term variability in the region. In the IMPROVE

212 program, elemental analysis was performed on the Teflon filters using X-ray fluorescence (XRF),

213 anions were analyzed using ion chromatography (IC), elemental carbon (EC) and organic carbon

214   (OC) were analyzed using a carbon analyzer (Hand, 2023). Chemical concentrations in the $PM_{2.5}$

215   fraction of nineteen elements (Al, As, Br, Ca, Cl, Cr, Cu, Fe, K, Mg, Mn, Na, Ni, Pb, Se, Si, Ti, V,

216   and Zn), along with nitrate, sulfate, elemental carbon (EC), organic carbon (OC), and calculated

217   coarse mass concentrations (PM_{10}−$PM_{2.5}$ mass concentrations), from January 2014 to April 2024

218   were used as input for the PMF analysis performed using EPA PMF 5.0 (Norris et al., 2014).

219   IMPROVE species concentrations were reported based on local conditions.

220   A five-factor solution was selected as the optimal solution based on the Q/Q_{exp} value and

221   interpretation of the physical meanings of the factors (Brown et al., 2015). The corresponding

222   factor profiles and time series are shown in Figures S5 and S6. These factors were identified, based

223   on chemical signatures and previous literature, as coarse dust, fine dust, biomass burning, sulfate-

224   dominated, and nitrate-dominated sources. Coarse and fine dusts had high contributions from Al,

225   Ca, Fe, Mg, and Si, which are the main components of mineral dust (Liu and Hopke, 2003). Coarse

226   dust explained more than 90% of the coarse mass ($> PM_{2.5}$), while there was no contribution from

227   coarse mass in the fine dust factor. The biomass burning factor was strongly associated with

228   organic and elemental carbon, which are mainly from combustion processes, and K, a tracer of

229   biomass burning (Hopke et al., 2020). The other two factors are dominated by nitrate and sulfate,

230   which are related to the formation of secondary aerosols and possibly some primary emissions

231   from regional sources that include energy production and distant urban regions. Some similar

232   factors were also resolved in published PMF analyses using IMPROVE data (Liu and Hopke, 2003;

233   Hwang and Hopke, 2007). Further details on the PMF analysis and results, as well as support for

234   their applicability over the broad surrounding Rocky Mountain region (IMPROVE sites at Mount

235   Zirkel and Rocky Mountain National Park) are provided in Supplement Text S1 and Figure S7.

236   Data for the PMF results are available through the ARM data product (Zhou et al., 2025a).

237   To assess the impact of different sources on INPs, the INP samples were categorized into six types

238   based on the dominant aerosol sources during the sampling period, and the contribution of sources

239   to each sample was shown in Figure S8. However, IMPROVE samples were taken only one of

240   every three days. For days without available IMPROVE data, aerosol sources were inferred from

241   the nearest sampling days. Samples were classified as follows: (1) Coarse dust, if coarse dust

242   contributed more than 50% to the total PM_{10} mass concentration or contributed more than 40%

243   and represented the largest contribution among all sources; (2) Biomass burning, if biomass

244   burning accounted for more than 50% of the total PM_{10}; (3) Dust, if the combined contribution of

245   coarse and fine dust exceeded 50% of the total PM_{10}, with the difference between fine and coarse

246   dust being less than 20%; (4) Fine dust, if the combined mass contribution of coarse and fine dust

247   exceeded 50% of the PM_{10} and fine dust exceeded coarse dust by more than 20%; (5) Mixed

248   samples, samples for which no single source was dominant, typically characterized by a sulfate

249   contribution greater than 20% of the PM_{10}. (6) Additionally, seven samples fell within periods

250   where more than one consecutive IMPROVE sample was missing (one week or longer). For these

251   cases, source contributions were not interpolated, and they were categorized as samples with no

252   source data. Source influences inferred from the nearest sampling days may introduce uncertainties.

253   However, the merged size distribution data (section 2.5 and Figure 2) for these days showed similar

254   size distribution patterns and comparable number concentrations for most size ranges compared to

255   the nearest days, suggesting that significant changes in aerosol sources for these inferred days were

256   limited. Also, the discussion is based on each group containing multiple samples, which should

257   also reduce the uncertainties associated with the inferred source from a single sample.

258

259   **2.4 Back trajectory analysis**

260   Air mass back trajectory analysis was performed using the Hybrid Single-Particle Lagrangian

261   Integrated Trajectory model (HYSPLIT; Stein et al., 2015; Rolph et al., 2017), developed by the

262   National Oceanic and Atmospheric Administration (NOAA) Air Resources Laboratory. For each

263   hour during each sampling period (typically 24 h), a 96-hour back trajectory was initiated at the

264   SAIL sampling site, starting 100 m above ground level, and using the GDAS meteorological

265   dataset with model vertical velocity. The areas traversed by the back trajectory were gridded into

266    $1° × 1°$ cells. For each trajectory, its occurrence in each grid cell was weighted by the residence

267   time spent in that cell. To account for the peak in occurrence near the sampling site, the residence

268   times were further normalized by the distance from the SAIL sampling site, following the method

269   of Ashbaugh et al. (1985). The analysis was performed for each sample, and the resulting

270   trajectories were aggregated to produce a composite residence-time map (Figure 1). Separate

271   analyses were also performed for samples categorized by different source types (Figure S9),

272   aggregating hourly trajectories for all sample times of a corresponding type across the campaign.

273   Back trajectory data are available through the ARM data product (Zhou et al., 2025b).

274

275   **2.5 Merged particle number-size distribution and IN active surface site density**

276   During the SAIL campaign, a scanning-mobility particle sizer (SMPS) and an optical particle

277   counter (OPC) were deployed simultaneously with the filter sample collection to measure aerosol

278   number size distributions in the particle diameter ranges from 10–500 nm and 0.25–35 μm,

279   respectively (Kuang et al., 2024; Cromwell et al., 2024). To obtain a continuous number size

280   distribution from 10 nm to tens of micrometers, measured number size distributions from the

281   SMPS and OPC were merged following previous methods (Hand and Kreidenweis, 2002;

282   Marinescu et al., 2019). Briefly, the mobility diameters from the SMPS were assumed to be equal

283 to volume equivalent diameters by assuming the particles are spherical, and number distributions

284 were converted to volume distributions. A scaling factor was determined by comparing the

285 overlapping size range of the two instruments, and the OPC volume size distribution was then

286 aligned with the SMPS volume distribution measurements by shifting OPC measured diameters to

287 estimate the SMPS mobility diameter corresponding to that optical diameter. All aerosol data from

288 the ARM archive were corrected to standard temperature (273.15 K) and pressure (101.3 kPa). All

289 merged size distribution data are available through the ARM data product (Zhou et al., 2025c). A

290 timeline of the merged number-size distributions of aerosols during the SAIL campaign is shown

291 in Figure 2.

292 Assuming that the number of active ice nucleation sites is linearly proportional to the particle

293 surface area, the IN active surface site density (m^{-2}) at temperature T (n_s(T), m^{-2}) was calculated

294 using the following equation:

$$n_{s,500}(T) = \frac{n_{\text{INP}}(T)}{S_{\text{m},500}} \times 10^9$$

295

296 where n_{INP}(T) (sL^{-1}) is the measured INP concentration at temperature T, $S_{\text{m},500}$ (µm^2/scm^3) is the

297 surface area concentration of particles larger than 500 nm diameter calculated from the merged

298 size distribution, assuming that particles are spherical, and the 10^9 conversion factor is used for

299 $n_{s,500}$ units of m^{-2}. In this study, the surface area of particles > 500 nm is used to exclude surface

300 area associated with pollution and other aerosol types that are inefficient sources of INPs. This is

301 supported by the correlation found between INP concentrations and the number concentrations of

302 particles > 500 nm in a previous study (DeMott et al., 2010). The n_s is also calculated based on

303 total surface area concentrations to facilitate comparison with other studies and is shown in Figure

304 S10. While the IN active surface site density approach is typically fully justified for single INP

305 compositions, we will apply it here to the total surface areas, but also discuss adjustments needed

306 when comparing to more specific INP parameterizations.

307

308 **3. Results and Discussion**

309 **3.1. INPs concentrations at the SAIL study site**

310 Samples not affected by artificial INP generation activities (cloud seeding and snowmaking

311 activities in winter; see section 2.2), representing the natural INPs in this region (84 samples in

312 total), are shown in Figure 3a. The discussion in this study focuses on these samples to better

313 understand the characteristics of natural INPs in the Rocky Mountain region. INP concentrations

314 ranged from 4×10^{-4} L^{-1} to 1.5 L^{-1} (mean: 0.15 L^{-1}, median: 0.05 L^{-1}) at -15 °C, and from 1.2

315 L^{-1} to 90 L^{-1} (mean: 16 L^{-1}, median: 12 L^{-1}) at -25 °C. This is comparable to online INP

316 measurements in the Rocky Mountain region (median: 8.2 L^{-1} at -26 °C; Lacher et al., 2025).

317 Compared with previous INP studies summarized by Kanji et al. (2017), the INP concentrations

318 observed during the SAIL campaign fall within the range of those in their compilation that were

319 influenced by dust, biomass burning, and precipitation, and are higher than those from marine

320 aerosols but lower than the maximum of those attributed to biological sources. Regarding temporal

321 variations, INP concentrations at all measured temperatures followed a similar trend over the

322 nearly two-year observation period: low in winter, increasing in spring, and reaching highest

323 concentrations during summer and early fall. For activation temperatures warmer than -25 °C, the

324 highest INP concentrations were all observed in summer. For temperatures colder than -25 °C, the

325 samples from summer also showed high INP concentrations, while the peak concentrations

326 occurred in September 2021. Back trajectories of those samples (2021-9-9 and 2021-9-16) showed

327 that the air masses mainly originated from the northwestern U.S. Intense wildfires occurred in that

328 region during the summer of 2021 (Jain et al., 2024), and the transported smoke plumes increased

329 aerosol loading at the SAIL site. These smoke intrusions may also result in enhanced INP

330 concentrations active at low temperatures.

331 Monthly mean INP concentrations were calculated and are presented in Figure 3b, to better

332 visualize seasonal trends and reduce the impact of individual outliers. INP concentrations showed

333 clear seasonal variations throughout the campaign. Note that our sampling did not cover the entire

334 month, so some outliers may have been coincidently captured or missed, however, the two-year

335 monthly dataset is still expected to broadly represent the seasonal variations of INPs in this region.

336 In general, INP concentrations reached peaks in June 2022 across all temperatures, and reached

337 minimum levels during winters in both years. However, differences existed among activation

338 temperatures. At warmer temperatures (−10 °C and −15 °C), INP concentrations were relatively

339 similar in warm seasons (April–October) and much higher than those in cold seasons (November–

340 March). Bioaerosols are typically recognized as major INP sources at these activation temperatures

341 (Kanji et al., 2017), and their emissions generally decrease in winter in most areas due to reduced

342 biological activities and possible snow cover limiting resuspension (Fröhlich-Nowoisky et al.,

343 2016). A distinct high INP peak was observed in June 2022, which was ten times higher than that

344 in June 2023, and much higher than in other months, suggesting that a high INP emission event

345 occurred during this month, which may be related to a specific biological emission event and/or

346 dust event. For activation temperatures of −20 °C and −25 °C, INP concentrations also showed a

347 seasonal pattern increasing from April, peaking in June, then decreasing and reaching a minimum

348 in December. Recent online INP measurements for activation temperatures from −22 °C to −32 °C

349 conducted from October 2021 to May 2022 and January to May 2025 at the Storm Peak Laboratory

350   in the Rocky Mountains (Lacher et al., 2025) found a similar seasonal pattern, with the lowest INP

351   concentrations in winter and increased in spring, suggesting that the INP sources could be similar

352   and may dominate INPs across a broaden region of the Rocky Mountains. The elevated INPs from

353   April to September may be attributed to enhanced dust aerosols, as dust concentrations were found

354   to increase during this period (Hand et al., 2017), and dust is a significant source of INPs,

355   especially at temperatures below −15 ℃ (Kanji et al., 2017; DeMott et al., 2015). Lower-

356   temperature INP concentrations in June 2022 were also higher than that those in June 2023, while

357   the magnitude of this difference (a factor of two) was less distinct from the difference at −10 ℃

358   (twelve times). This suggests that the origins of INPs activated at lower temperatures differ from

359   those at warm temperatures.

360

361   **3.2. Relationships between aerosol sources and INPs**

362   The sources of aerosols to the SAIL campaign region were identified based on the PMF analysis

363   (Text S1, Figures S5 and S6). Different sources exhibited unique seasonal trends. Coarse dust

364   showed increased concentrations from April to September and had the highest annual mean

365   concentration among the five resolved particle types. Fine dust increased sharply in April, May,

366   and June, and remained low during other months. Biomass burning aerosol varied significantly by

367   year. Strong peaks in concentrations were observed in September 2021, with SAIL collecting some

368   samples at the end of these events, and increased contributions in June–August 2022. The biomass

369   burning factor typically showed high concentrations in summer. The sulfate-dominated and nitrate-

370   dominated factors had much lower concentrations overall, with peaks occurring in summer and

371   spring, respectively. The aerosol number size distribution also reflected the variations in different

372   sources (Figure 2). Supermicron particle concentrations were higher when coarse dust increased.

373   Submicron particles concentrations increased in September 2021 and the summer of 2022, which

374   corresponded to increases in contributions from the biomass burning factor. To investigate the

375   impact of different aerosol types on INPs, temporal variations between aerosol sources and INP

376   concentrations at −15 °C and −25 °C were compared, as shown in Figure 4. Monthly average

377   concentrations were used to minimize the impact of unsampled dates. Although this may introduce

378   uncertainties by smoothing episodic peaks of a source, the nearly two-year (22 months) record

379   should adequately represent its seasonal cycle. Pearson correlation coefficients between monthly

380   INP concentrations (−10 °C, −15 °C, −20 °C, and −25 °C) and aerosol sources are shown in Table

381   1.

382   Coarse dust and biomass burning presented seasonal variations similar to those of INPs at −15 °C

383   and −25 °C, while fine dust, nitrate-dominated, and sulfate-dominated factors had weaker

384   correlations (Figure 4). The strong correlations with coarse dust and biomass burning aerosols

385   suggest that these sources significantly contributed to observed INPs. Coarse dust showed good

386   correlations with INPs active at all temperatures (Table 1), with correlation coefficients increasing

387   for colder temperatures, suggesting that coarse dust is a major source of INPs, particularly at lower

388   temperatures. This is consistent with previous findings that dust dominates the INPs at

389   temperatures below −20 °C (Beall et al., 2022; Testa et al., 2021; Kanji et al., 2017). Furthermore,

390   Lacher et al. (2025) provided direct evidence that INPs active at cold temperatures were

391   significantly contributed by supermicrometer particles, which they attributed to dust, in the Rocky

392   Mountains. Their observation site was located near to the IMPROVE site at Mount Zirkel, where

393   our PMF analyses identified similar sources and trends to those near the SAIL (Text S1),

394   suggesting that INPs in both studies were impacted by coarse dust. Interestingly, coarse dust

395   presented a weaker correlation with INPs at −10 °C ($R^2 = 0.43$), a temperature range usually

396   associated with biological INPs. This may be due to the large number of coarse dust particles,

397   biological INPs carried on dust particles, and/or the inclusion of biological particles in the coarse

398   dust factor, as biological particles are mostly supermicron in size (Després et al., 2012). Biomass

399   burning presented a strong correlation with INP at −25 °C and weak correlations at warmer

400   temperatures (−10 °C and −15 °C), suggesting that aerosols from biomass burning contribute

401   primarily to INPs active at lower temperatures. Combining coarse dust and biomass burning

402   contributions showed an even better correlation with INPs (Table 1), supporting that these are the

403   major contributors of INPs in this region, especially at lower activation temperatures.

404   Different from coarse dust, fine dust showed weak relationships with INPs at all temperatures (R^2

405   = 0.10–0.19), suggesting lower contributions to INPs. One possible reason is that larger particles

406   have more ice nucleation active sites (Reicher et al., 2019; DeMott et al., 2010). Another reason

407   could be differences in sources of fine and coarse dust that resulted in different ice-nucleating

408   abilities. Fine dust presented a different seasonal pattern compared to coarse dust. Fine dust

409   concentrations peaked in spring, especially in April, while coarse dust was higher in summer. This

410   difference was also observed in Hand et al. (2017) for the Colorado Plateau and Central Rockies

411   regions. They suggested that fine dust in this region is influenced by regional or long-range

412   transported dust, such as Asian dust, while coarse aerosol mass concentrations (defined as the

413   difference between PM_{10} and $PM_{2.5}$, which was almost all loaded into the coarse dust factor in our

414   PMF analysis) are mainly derived from local and regional sources. Sulfate-dominated and nitrate-

415   dominated sources were not correlated with INP concentrations. In remote areas, sulfate and nitrate

416   particles mainly come from secondary formation (Seinfeld and Pandis, 2016) and are generally

417   not considered as efficient INPs (Kanji et al., 2017).

418

3.3. INP temperature spectra categorized by sources

The total INP temperature spectra categorized by dominant aerosol types are shown in Figure 5a, and total INP spectra sorted under dominant influence of each source type are plotted separately in Figure S11. Significant differences in INP concentrations were observed between periods where different aerosol source types were dominant. Over 50% of the samples were dominated by coarse dust, which was the predominant aerosol source in this region (Figure S8). Considering that coarse dust also showed a strong correlation with INPs, this suggests INP concentrations were likely primarily influenced by coarse dust in this area. Mineral dust (DeMott et al., 2003; Niemand et al., 2012; Atkinson et al., 2013), soil dust that contains abundant organics (Tobo et al., 2014; Steinke et al., 2016; O'Sullivan et al., 2014), and playa dusts (Pratt et al., 2010; Hamzehpour et al., 2022) have been widely investigated, and are considered as important INP sources. Based on back trajectories for samples categorized as coarse dust-dominated (Figure S9), air masses were mostly from local or regional sources (Central Rockies and Colorado Plateau, with additional inputs from the agricultural Imperial Valley in southern California). Considering their larger size and mass, coarse dust particles have relatively short atmospheric transport ranges, and local resuspension of soil is likely a dominant source (Hand et al., 2017). High air mass residence times were also indicated for the Great Salt Lake region, suggesting potential contributions from playa salts. This is consistent with the contributions of Cl and Na in the coarse dust factor profile from the PMF analysis (Figure S5a), and playa salt dusts have also been observed, at least at lower temperatures in the mixed phase regime, to serve as INPs (Pratt et al., 2010; Koehler et al., 2007).

Compared to INPs samples that aerosols dominated by coarse dust, fine dust-dominated time periods showed lower INP concentrations (Figure 5). Back trajectories also indicated different origin regions from those for coarse dust; samples dominated by fine dust had trajectories mainly

442 from southern California and the Sonoran Desert in Arizona, known as an area with high dust

443 emissions (Ginoux et al., 2012). Fine dust is likely long-range transported as Asian dust (Hand et

444 al., 2017) or from the noted southwestern desert areas. Besides their different origins, the higher

445 INP concentrations associated with coarse dust-dominated samples compared to those dominated

446 by fine dust can also be attributed to differences in particle size, although confirming this would

447 require data on size-resolved INPs that were not collected. INPs related to biomass burning-

448 dominated samples presented comparably high concentrations, which may be related to the

449 significantly elevated aerosol loading during biomass burning events. To assess the ice nucleating

450 activity, with the influence of aerosol concentrations and size distributions accounted for, the IN

451 active surface site density was further investigated.

452

3.4. IN active surface site density (n_s) temperature spectra

454 The IN active surface site density (n_s) temperature spectra, a measure of INPs per aerosol surface

455 area, are shown in Figure 5b for all samples, categorized by dominant aerosol type. Compared to

456 INP concentrations, the n_s values were less variable at a given temperature, with most samples

457 within one order of magnitude of each other, whereas INP concentrations spanned nearly two

458 orders of magnitude, suggesting that at least some of the variability in INP concentrations can be

459 explained by differences in particle size distributions and concentrations.

460 Samples dominated by a specific aerosol source (coarse dust, dust, fine dust, or biomass burning)

461 exhibited relatively consistent n_s values with some differences among categories. The n_s of samples

462 dominated by coarse dust was similar to or slightly higher than those having both abundant coarse

463 and fine dusts (categorized as dust), suggesting that INPs from coarse dust have higher IN active

464 surface site density. After normalizing by surface area, the n_s for the fine dust-dominated samples

465 showed closer values with those of the coarse dust-dominated samples, while still lower. This

466 suggests that the lower INP concentrations in fine dust-dominated samples can be partly attributed

467 to differences in aerosol surface area concentrations, but also to lower active site density due to

468 potentially different INP sources. The differences in n_s between coarse dust- and fine dust-

469 dominated samples were limited, likely because there were still small contributions from coarse

470 dust (17% on average), although fine dust dominated these samples (59% on average).

471 During biomass burning events, aerosol number concentrations were significantly enhanced,

472 especially for submicron particles (Figure 2). A correlation was found between the biomass

473 burning factor mass concentrations and the total surface area concentrations of aerosols (Figure

474 S12), suggesting that such events significantly increased aerosol surface area concentrations.

475 However, its contributions to INPs could be affected by coarse dust. After normalization by surface

476 area ($S_{m,500}$), the n_s of INP samples for aerosols dominated by biomass burning were similar to

477 those of coarse dust-dominated samples. Compared with previous studies (comparison based on

478 computing n_s using total surface area), these values were higher than n_s reported from laboratory

479 biomass burning studies (Umo et al., 2015; Jahn et al., 2020) and those reported in ambient biomass

480 burning observations (McCluskey et al., 2014; Barry et al., 2021b; Zhao et al., 2024). During SAIL,

481 this finding may have been due to the presence of coarse dust, which has a much higher n_s than

482 biomass burning, as this aerosol type still contributed moderately to the total aerosols in these

483 samples (an average of 22% of PM_{10}), although biomass burning was the dominant aerosol source

484 (62% on average). Wildfire events could also be a source of airborne dust (Wagner et al., 2018;

485 Meng et al., 2025). From the NOAA Hazard Mapping System (Figure S13) and back trajectories

486 (Figure S9), these samples were mostly affected by long-range transported biomass burning

487 aerosols originating primarily from wildfires in the northwest and southwest U.S. Aging could

488 enhance the n_s of biomass burning INPs (Jahl et al., 2021) and may also have contributed to higher

489 n_s of these samples.

490 In contrast to the convergence observed in samples dominated by a single source, samples related

491 to mixed sources showed no reduction in variability after normalization by surface area (Figure 5

492 and Figure S11). Although it is difficult to precisely determine the INP sources for these samples

493 based on current available analyses, this comparison strongly supports the link between INPs and

494 the dominant bulk aerosol sources in this study.

495

496 **3.5 Evidence of biological contribution to INPs**

497 From the INP temperature spectra and n_s for all samples (Figure 5), the spectra for INPs active at

498 temperatures higher than about −18 °C showed a segregation into two groups: one with higher INP

499 concentrations (and n_s) and measured detectable freezing onset temperatures mostly > −10 °C, and

500 the other with lower INP concentrations (and n_s) and lower measured detectable freezing onset

501 temperatures, with most of those samples assigned to aerosol sources of mixed and fine dust. We

502 found all samples in the latter group were collected from December to March. At freezing

503 temperatures warmer than −15 °C, biological INPs are likely to play a more important role (Kanji

504 et al., 2017).

505 Here, we separated samples collected during cold seasons (December–March) and during other

506 seasons (April–November), as shown in Figure 6. This separation clearly shows that on average,

507 INP concentrations were lower in cold seasons, with the most striking difference at temperatures

508 warmer than −15 °C (15% of INPs in other seasons). A further comparison of n_s (Figure 6b) showed

509   that samples from cold seasons had similar n_s at temperatures colder than around −18 ℃. However,

510   at warmer temperatures, samples from cold seasons showed consistently lower n_s. These results

511   suggest that INPs that activated at temperatures colder than around −18 ℃ likely originated from

512   similar sources throughout the whole year, which were primarily associated with coarse dust, as

513   discussed above. However, in cold seasons, the contribution from biological INPs was

514   significantly reduced, leading to the divergence in the spectra for temperatures warmer than around

515   −18 ˚C. This seasonal pattern is supported by the environmental temperature dependence of

516   biological aerosol emissions (Shawon et al., 2025).

517   The likely biological nature of these warmer-temperature INPs was also identified from the heat

518   treatment of samples. A compilation of spectra from all base (untreated) analyses, heat, and H_2O_2

519   treatments is shown in Figure 7. The difference between the base and heat spectra indicated a large

520   contribution (82–94%, 90% on average) of heat-labile INPs at warm temperatures (> −15 ℃),

521   which are presumably biological INPs. Each individual heat spectrum is shown in Figure S1. In

522   September 2021, most samples showed decreased INP concentrations at temperature warmer than

523   −15 ℃ after heat treatment, while almost no decrease was observed at lower temperatures. This

524   reduction is likely due to denaturing of biological INPs, reducing or removing their IN activity

525   (Hill et al., 2016). Samples from September 2021 were strongly affected by biomass burning

526   (Figure S6). Kobziar et al. (2024) found that biological aerosols can be co-emitted in biomass

527   burning. The presence of biological INPs in smoke plumes was also suggested in aircraft

528   measurements of biomass burning aerosols, which showed base and heat-treated spectra (Barry et

529   al., 2021b) similar to those observed in SAIL samples from September and October 2022. During

530   the SAIL campaign, Shawon et al. (2025) and Ashfiqur et al. (unpublished data) detected biological

531   aerosols using a Wideband Integrated Bioaerosol Sensor (WIBS) and scanning electron

microscopy during selected intensive observation periods (June–September 2022 and September 2022, respectively), further supporting the presence of biological aerosols during these periods, some of which may be active as INPs. Biological/heat-labile INPs during the cold seasons account for only 4% of those in the other seasons. There were no significant decreases in warm-temperature INP concentrations after heat treatment for samples collected from January to early April 2022 and December 2022 to March 2023, indicating that biological INPs concentrations were very low during the cold seasons. In the other seasons (April–November), many samples showed spectra in which heat treatment significantly decreased INP concentrations at temperatures > −15 ℃ and almost no change at lower temperatures, suggesting abundant heat-labile INPs, presumably of biological origin.

3.6 Relationships among INPs types inferred from treatments

After H_2O_2 treatment, almost all samples showed significant decreases (83–97%, with an average reduction of 91%)) in INP concentrations across all measured activation temperatures (Figure 7 and Figure S2), suggesting substantial contributions from organic INPs through the entire temperature spectrum. The inorganic INPs and other organic INPs were correlated at −15 ℃ and −25 ℃ (Figure 8e and 8f), especially at the lower temperature. The correlations clustered around the 10:1 line, with ratios of 14 and 13 at −15 ℃ and −25 ℃, respectively. These results indicated a dominant contribution from organic components suggestive of a soil origin, as previous studies found that soils contain abundant organic INPs in addition to mineral INPs (Tobo et al., 2014; O'Sullivan et al., 2014; Pereira et al., 2022; Suski et al., 2018; Testa et al., 2021). A short-term observational study (DeMott et al., 2025) at the Storm Peak Laboratory in the Colorado Rockies also attributed soil INPs as the dominant INP source in late summer and early fall. These

correlations provide further support that the coarse dust factor was mainly from resuspension of local or regional soil dust. Testa et al. (2021) also found a correlation at −25 °C between other organic and inorganic INPs, with a mean ratio of 5.5 in samples from north-central Argentina. Our results and those of Testa et al. (2021) suggest that other organic INPs and inorganic INPs are co-emitted from similar sources. The correlation coefficient increased at lower temperatures, possibly because other organic and inorganic INPs had limited contributions at −15 °C, a range strongly influenced by biological aerosols. Note that INPs from biomass burning could also contribute to this correlation, as they show similar organic and inorganic INP characteristics in their INP spectra (Schill et al., 2020; Barry et al., 2021b). The only exception is sample 2021-10-14, for which similar INP concentrations were observed in the base, heat, and H_2O_2 treatments at temperatures < -15 °C, suggesting that it was likely dominated by mineral dust.

Unexpectedly, a correlation was observed between the biological/heat-labile INPs and other organic INPs at −15 °C ($R^2 = 0.61$, n = 29, Figure 8a). This correlation suggests that increases in heat-labile INPs, presumably biological INPs, were accompanied by increases in organic INPs. This is possibly because both biological and organic INPs during SAIL originated from the same source at this temperature, which was likely soil dust. However, at a warmer temperature (−12.5 °C), the correlation was weaker ($R^2 = 0.10$, n = 20), possibly because biological INPs from non-soil sources contributed at higher temperatures (Huang et al., 2021), as the ratios between biological/heat-labile INPs and other organic INPs changed from 13 (−15 °C) to 43 (−12.5 °C). At −25 °C, correlations between biological/heat-labile INPs and other organic INPs were much weaker, and the ratio was much lower (mean ratio of 2).

3.7 Prediction of INPs in the Rocky Mountain region

578   In this study, n_s values were found to be close to those used in the parameterizations derived from

579   studies of agricultural soil (Tobo et al., 2014), desert dust (Niemand et al., 2012), and fertile soil

580   (O'Sullivan et al., 2014) (Figure S14a). Applying the parameterization from Tobo et al. (2014)

581   using the surface area of particles > 500 nm reasonably estimated INP concentrations (Figure

582   S14b), but tended to underestimate them. This is possibly because the equation provided by Tobo

583   et al. (2014) requires an estimation of the surface area of soil particles, which introduces

584   uncertainties when using $S_{m,500}$; accurately estimating surface area of only soil particles in

585   atmospheric samples requires additional analysis. Also, the equation from Tobo et al. (2014) is not

586   valid for T > −18 ℃. The parameterization from O'Sullivan et al. (2014) includes a wider

587   temperature range, while it tended to underestimate in temperatures warmer than −20 ℃ and

588   overestimate at colder temperatures (Figure S14b). The parameterization from Niemand et al.

589   (2012) was derived from desert dust, consisting mainly of mineral dust. Some of their dust samples

590   might have contained arable dust or biological INPs (Beall et al., 2022). Application of their

591   parameterization to our data showed a bias at warm temperatures (Figure S14b). Therefore, we

592   developed a parameterization based on the SAIL samples, which could be useful for estimating

593   atmospheric INPs dominated by organic-containing soil dust.

594   Parameterization was based on an assumed relationship between IN active surface site density (n_s,

595   m^{-2}) calculated from surface area concentrations of particles > 500 nm ($S_{m,500}$) and temperature

596   (T, ℃) over all seasons. First, a single polynomial equation fitted to data from all samples was

597   obtained (Figure S15), and the INP concentrations predicted from this equation and the measured

598   $S_{m,500}$ were compared with the measured INP concentrations (Figure S15). The predicted INPs

599   were mostly within one order of magnitude of the measured values, suggesting this fit generally

600   provides a reasonable estimation of INPs. However, the predicted INPs showed an overestimation

601   trend for some samples around −15 °C. This is due to the limited contribution of biological/heat-

602   labile INPs in cold seasons.

603   To better represent the INP temperature spectra accounting for the seasonality of biological

604   contributions, parameterization equations were fitted as polynomials for samples from other

605   seasons (April–November, equation 1) and cold seasons (December–March, equation 2) separately

606   (Figure 9), as follows,

$$\ln(n_s) = -0.007T^2 - 0.785T + 6.636 \ (-30\ °C < T < -6\ °C) \qquad (1)$$

$$\ln(n_s) = -0.030T^2 - 1.833T - 5.076 \ (-20\ °C < T < -10\ °C) \qquad (2)$$

607   Equation 1 was derived for most samples except those from cold seasons, and Equation 2 was

608   obtained for samples from cold seasons (December–March). Equation 2 was constrained to

609   intersect with Equation 1 at −20 °C, as there were no significant differences at T < −20 °C, and

610   Equation 1 was used in this range. The agreement between predicted and measured INPs based on

611   these two equations showed improvement compared to using the one equation method above

612   (Figure S15), better representing the measured INPs across the full measured temperature range

613   (Figure 9). The accurate prediction of the nearly two years of observations of INPs using this single

614   parameterization, rather than requiring multiple n_s-based parameterizations for specific sources, is

615   likely due to the dominance of coarse dust as the primary INP source in this region. Note that the

616   lack of precise parameterization for biological INPs still introduces larger uncertainties in

617   predictions at warm temperature ranges, while applying the two-equation parameterization based

618   on the seasonal signature of biological INPs identified in this study improves the prediction.

619

620   **4 Summary and atmospheric implications**

621   This study comprehensively characterized INPs over a nearly two-year period in the mountainous

622   Upper Colorado River Basin region. The observed average INP concentrations were 0.15 L^{-1} at

623   −15 °C and 16 L^{-1} at −25 °C. Clear seasonal variations of INP concentrations and temperature

624   spectra were observed, with low concentrations in winter, increasing in spring, peaking in summer,

625   decreasing in autumn, and returning to low levels in winter. The aerosol types in this region were

626   identified as coarse dust, fine dust, biomass burning, sulfate-dominated, and nitrate-dominated.

627   Coarse dust concentrations were strongly correlated with INP concentrations in all seasons and

628   over a large temperature range, suggesting that background INPs in the study region were strongly

629   influenced by coarse dust. Further analysis of the IN active surface density site supported the

630   dominant role of coarse dust in INPs. Abundant organic INPs were identified, suggesting that

631   organic-containing soil dust was the primary source of INPs. Back trajectories showed that coarse

632   dust mostly originated from local or regional sources. This study also found clear evidence of

633   biological and heat-labile INPs, which showed strong seasonal dependence. Heat-labile,

634   presumably biological INPs were present during warm seasons but were significantly decreased

635   in winter. Two parameterization equations based on IN active surface site density were developed

636   for warm and cold seasons separately. These equations well estimated the measured INP

637   concentrations across the measured temperature and concentration ranges. The parameterization

638   developed here could be useful for representing INPs from organic-containing soil dust in other

639   mountain regions.

640   This long-term observation identified that organic-containing soil dust is the major source of INPs

641   in the Rocky Mountain region. Biomass burning aerosols and fine dust, likely from long-range

642   transport, play less important roles in INPs compared to coarse dust in this region. Our results

643   indicate that soil dust from nearby regions (e.g., the Colorado Plateau and Central Rockies), rather

644 than long-range transported fine and mineral dust, dominates contributions to the INPs in the

645 Upper Colorado River Basin, and therefore influences aerosol-cloud interaction and precipitation.

646 This study investigated the major INP sources by linking long-term INP measurements with

647 aerosol source apportionment, presenting reasonable results that agree well with other studies

648 (DeMott et al., 2025; Lacher et al., 2025). This approach may have broader applicability for INP

649 source attribution in other regions. Future studies combining short-term online INP measurement

650 (e.g., continuous flow diffusion chamber, CFDC) with detailed chemical analyses (e.g., mass

651 spectrometer) would be valuable for providing more direct evidence of INP sources, such as

652 demonstrated by the approaches used in Cornwell et al. (2023, 2024).

653 In this study, the origins of biological INPs are unclear due to the limitations of the analytical

654 methods used. One possibility is that biological INPs were associated with soil dust, e.g., fungi in

655 soil (Conen and Yakutin, 2018; O'Sullivan et al., 2016). This is supported by the correlation

656 between biological/heat-labile INPs and other organic INPs at $-15\,°C$. Also, raindrop impact could

657 be an important biological INP emission pathway (Prenni et al., 2013; Mignani et al., 2025). In

658 cold seasons, snow covers the Rocky Mountain region and inhibits the suspension of local soil

659 dust, which is considered as the main source of INPs in this region. This assumption that coarse

660 dust emissions are suppressed in cold seasons is also supported by the observation that more than

661 half of the samples in cold seasons were dominated by mixed sources and fine dust, instead of

662 coarse dust. However, the correlation between biological/heat-labile INPs and other organic INPs

663 was weaker ($R^2 = 0.10$) at a warmer temperature ($-12.5\,°C$). This suggests that there are

664 contributions from other biological INPs (e.g., those originating from vegetation) at warmer

665 freezing temperatures, which are likely independent of soil dust emissions, thereby complicating

666 the estimation of biological INPs. For example, airborne bacteria (Bowers et al., 2012) and pollen

667 (Fall et al., 1992) in the Rocky Mountain region decrease in winter and increase during the warmer

668 seasons. This seasonal pattern is consistent with the variation in biological/heat-labile INPs

669 observed in this study, suggesting that these biological particles may represent potential sources of

670 the biological INPs. In this case, the INP spectra in cold seasons likely represent that of soil dust,

671 and the spectra in other seasons represent the combination of soil dust and biological INPs. While

672 bacteria may also be partly related to soil, as summer bacteria taxa were reported to likely originate

673 from soil and leaf surface (Bowers et al., 2012), the specific ice-active taxa among them require

674 further investigation. In future studies, identifying the most abundant biological INPs in this region

675 and determining whether they originate from vegetation, soil-associated sources, or from a

676 combination of both would help improve our understanding of biological INP variability and

677 improve their estimation. However, besides heat treatment, current approaches provide only

678 indirect evidence of biological INPs (Cornwell et al., 2023 and 2024; Sanchez-Marroquin et al.,

679 2021). Comprehensive characterization of biological aerosol types and abundance, or developing

680 new analytical approaches, would be highly beneficial for advancing biological INP research.

681 The INP concentrations in this study were similar to those observed in ambient samples influenced

682 by agricultural soil in Argentina (Testa et al., 2021). The n_s values reported for agricultural soil

683 samples (Tobo et al., 2014) were higher than those calculated from total surface area (Figure S10),

684 but similar to n_s when based on surface area of particles > 500 nm (Figure S14). This finding

685 suggests that using particles > 500 nm is a reasonable threshold for excluding most aerosol types

686 that are inefficient INP sources, and approximating aerosol surface area contributions from

687 organic-containing soils. Since SAIL was conducted at a remote site in the Rocky Mountains, these

688 comparisons suggest that the parameterization developed in this study can potentially be applied

689 to other remote continental areas. A recent global modeling study (Herbert et al., 2025) found that

690   including organic INP components in dust particles, which are present in many soils, can

691   significantly improve predictive accuracy. It is therefore essential to validate the INPs originating

692   from organic-containing soil dust, beyond the mineral dust that has already been intensively

693   studied, through field measurements across different continental regions.

694

Data Availability

696   The data from the SAIL campaign used in this study are available through the ARM Data

697   Discovery (https://adc.arm.gov/discovery/). This includes INPs data (Shi et al., 2025), source

698   apportionment results (Zhou et al., 2025a), back trajectory data (Zhou et al., 2025b), merged

699   aerosol number-size distribution (Zhou et al., 2025c), and particle number size distribution data

700   from SMPS (Kuang et al., 2024) and OPC (Cromwell et al., 2024).

701

Author contributions

703   RP, SK, PD, and RZ conceptualized the study. DJ, RZ, KA, and OD performed additional

704   immersion-mode INP measurements. RZ, RP and SK conducted the source apportionment and

705   merged the size distribution data. RZ, RP, KA and SK performed the back trajectory analysis. KB

706   performed qPCR analysis. RZ wrote the manuscript, with revisions from RP, PD, and SK. All

707   authors reviewed the manuscript and contributed to the final version of the manuscript.

708

Competing interests

710   The authors declare no competing interests.
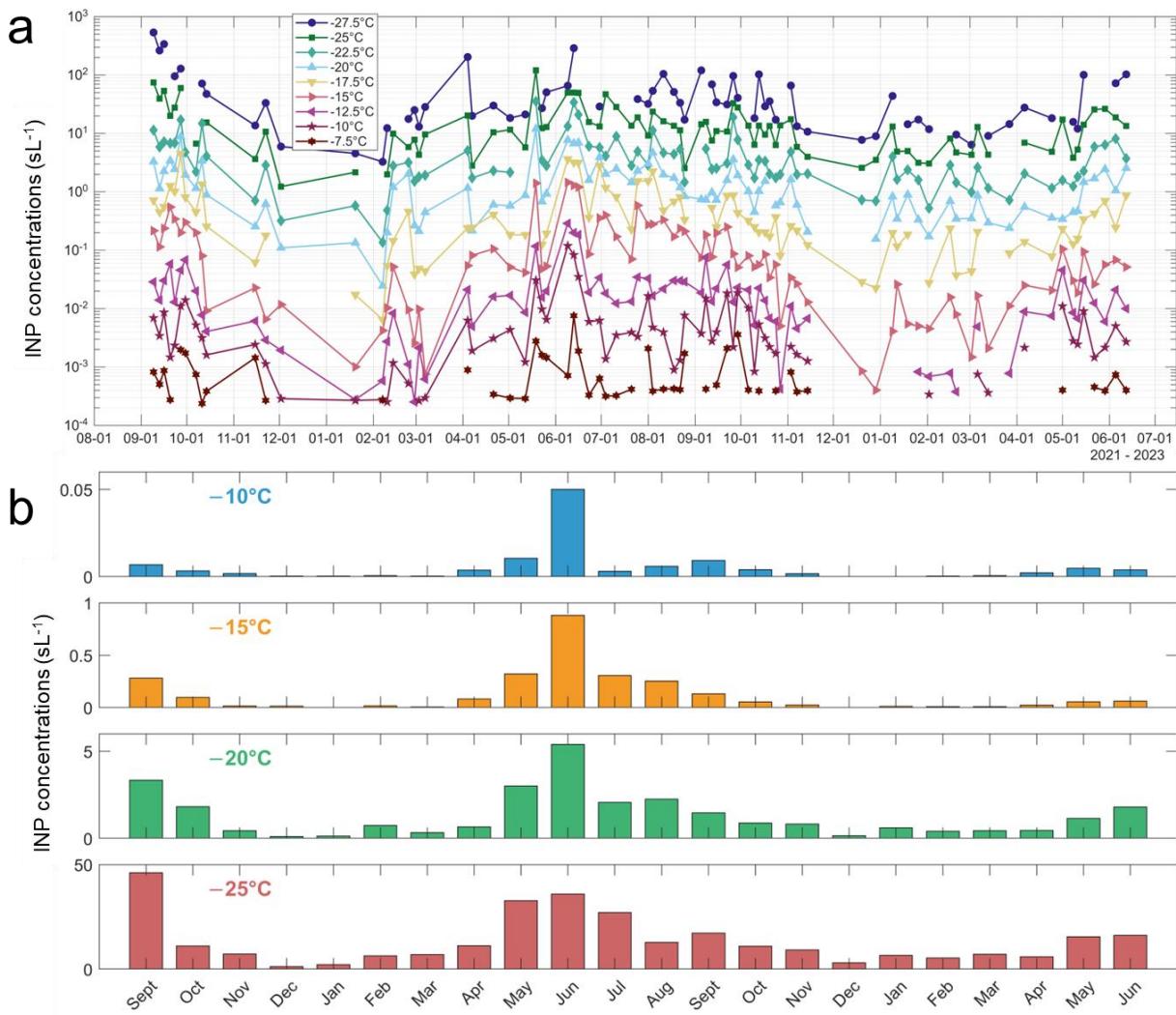
728

Figure 1. Residence-time weighted back trajectories for all sampling periods. 96-hour back trajectories were generated hourly during each sampling period and normalized by residence time and distance from the sampling site. The residence-time coefficients indicate the relative time air masses spent within each grid cell. The black star marks the SAIL sampling location.
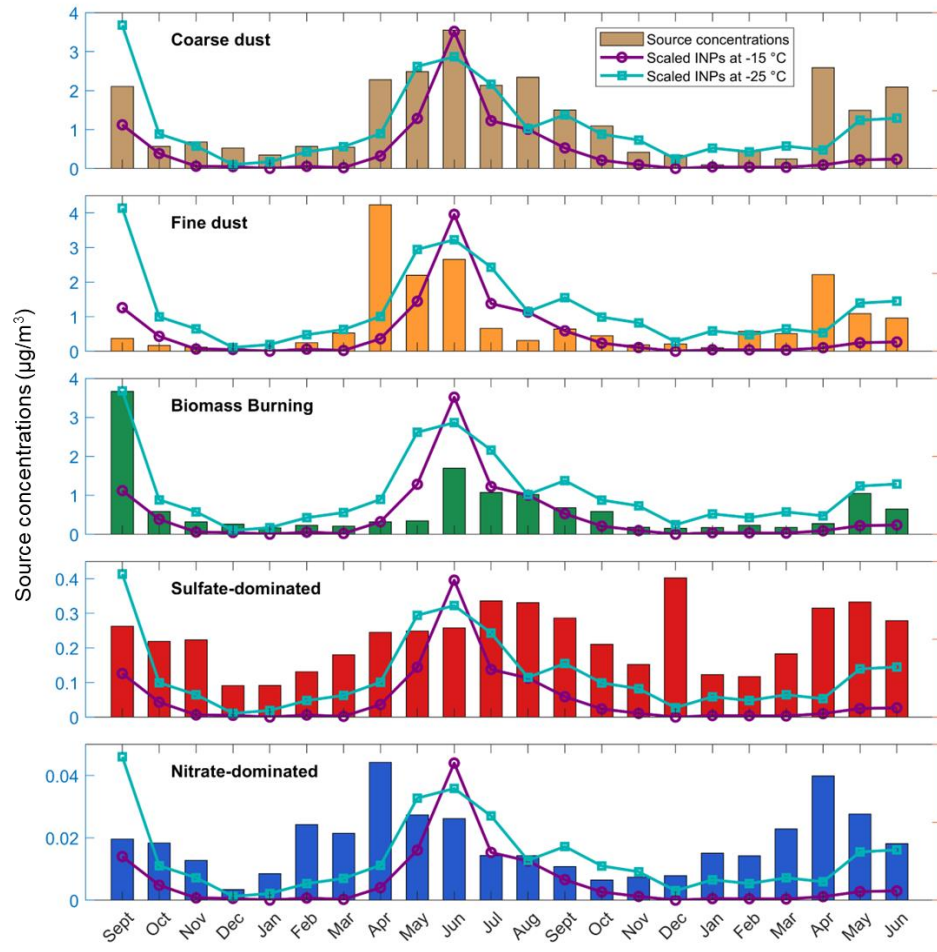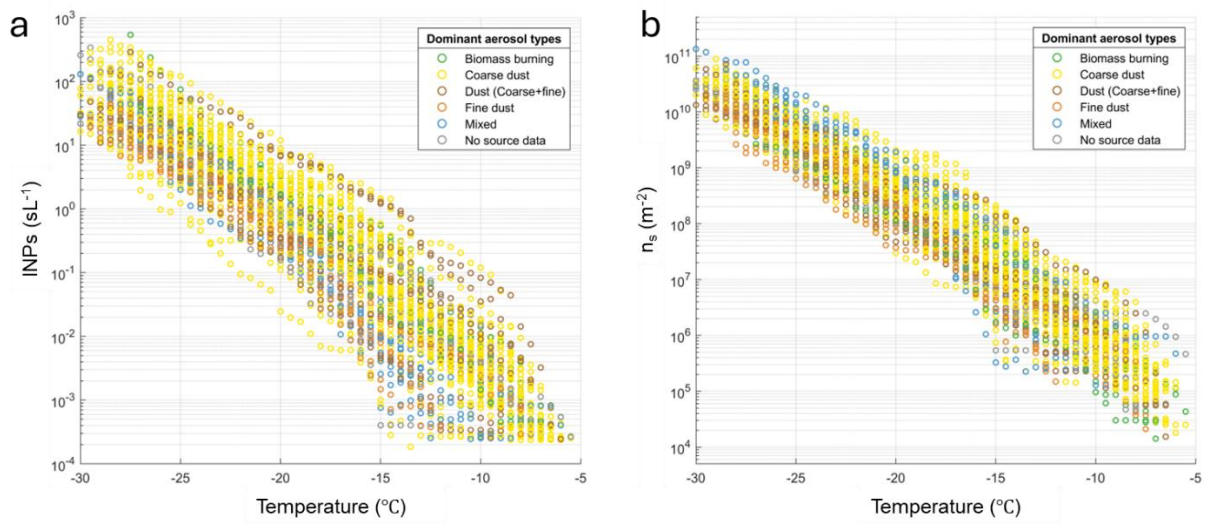
733

734

Figure 2. (a) Number size distribution ($dN/d\log D_p$, scm^{-3}), surface area size distribution ($dS/d\log D_p$, µm^2/scm^{-3}), and volume size distribution ($dV/d\log D_p$, µm^3/scm^{-3}), derived from merged size distribution assuming spherical particles during the SAIL campaign. (b) Time series of aerosol mass concentrations (µg m^{-3}) of coarse dust, fine dust, and biomass burning. Lines and bars represent daily and monthly mean concentrations, respectively.

Figure 3. Measured INP concentrations (sL^{-1}) during the SAIL campaign (September 2021–June 2023), excluding samples obtained during cloud seeding and snowmaking activities. (a) INP concentrations at temperatures from −7.5 °C to −27.5 °C in 2.5°C intervals. (b) Monthly mean INP concentrations at temperatures of −10 °C, −15 °C, −20 °C, and −25 °C.

Figure 4. Monthly mean INP concentrations (lines, arbitrary scaling) at −15 °C and −25 °C and monthly mean aerosol mass concentrations (bars) from coarse dust, fine dust, biomass burning, sulfate-dominated, and nitrate-dominated sources.
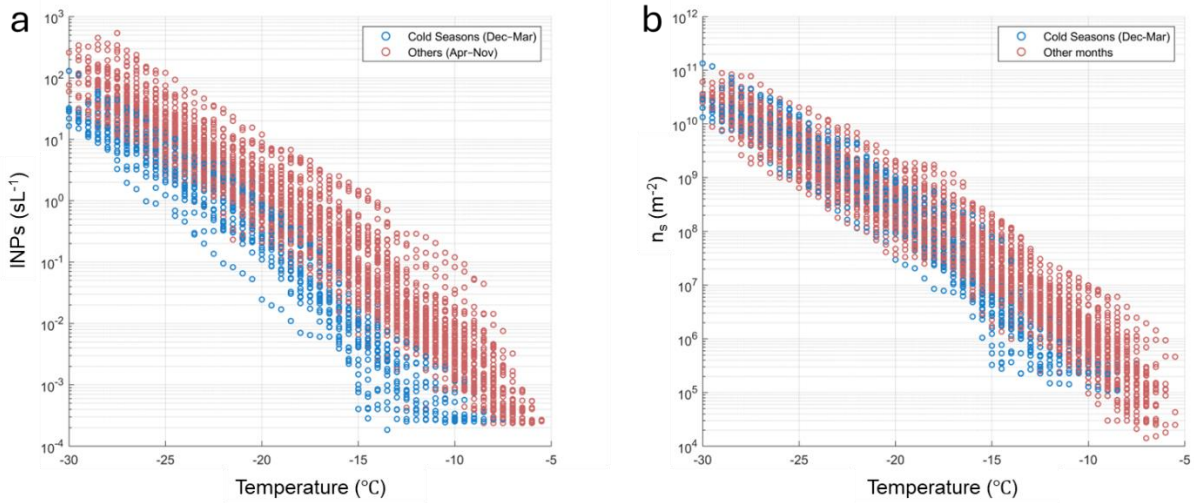
751

Figure 5. (a) Total INP concentration (sL^{-1}) temperature spectra, and (b) IN active surface site density (n_s, m^{-2}) calculated based on the surface area of particles larger than 500 nm. All samples were categorized by the dominant aerosol sources. Colors in the legend represent the dominant aerosol types during sampling.
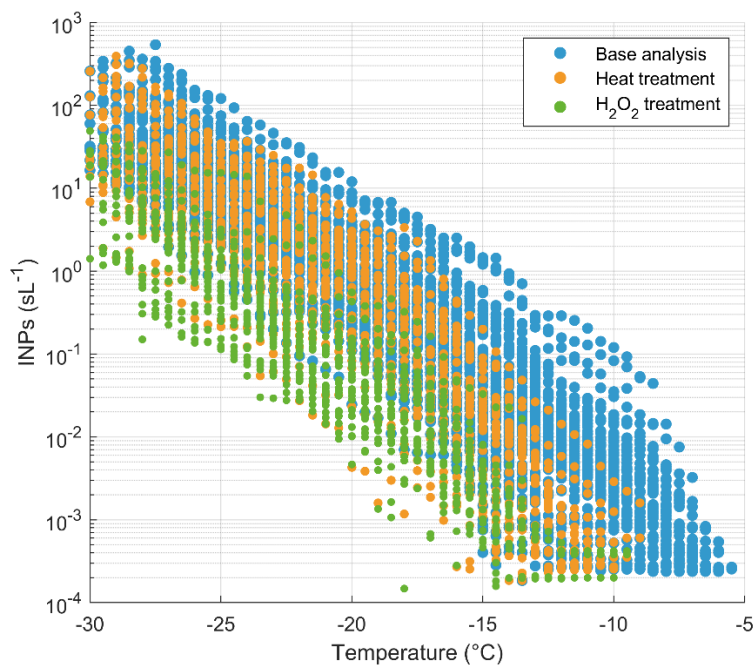
756

Figure 6. (a) INP temperature spectra and (b) IN active surface site density (n_s) categorized by sampling date as cold seasons (December–March) and other seasons (April–November). n_s was calculated based on the surface area of particles larger than 500 nm.

762

763   **Figure 7**. Comparison of INP temperature spectra from base (untreated), heat-treated, and H_2O_2-
764   treated analyses.
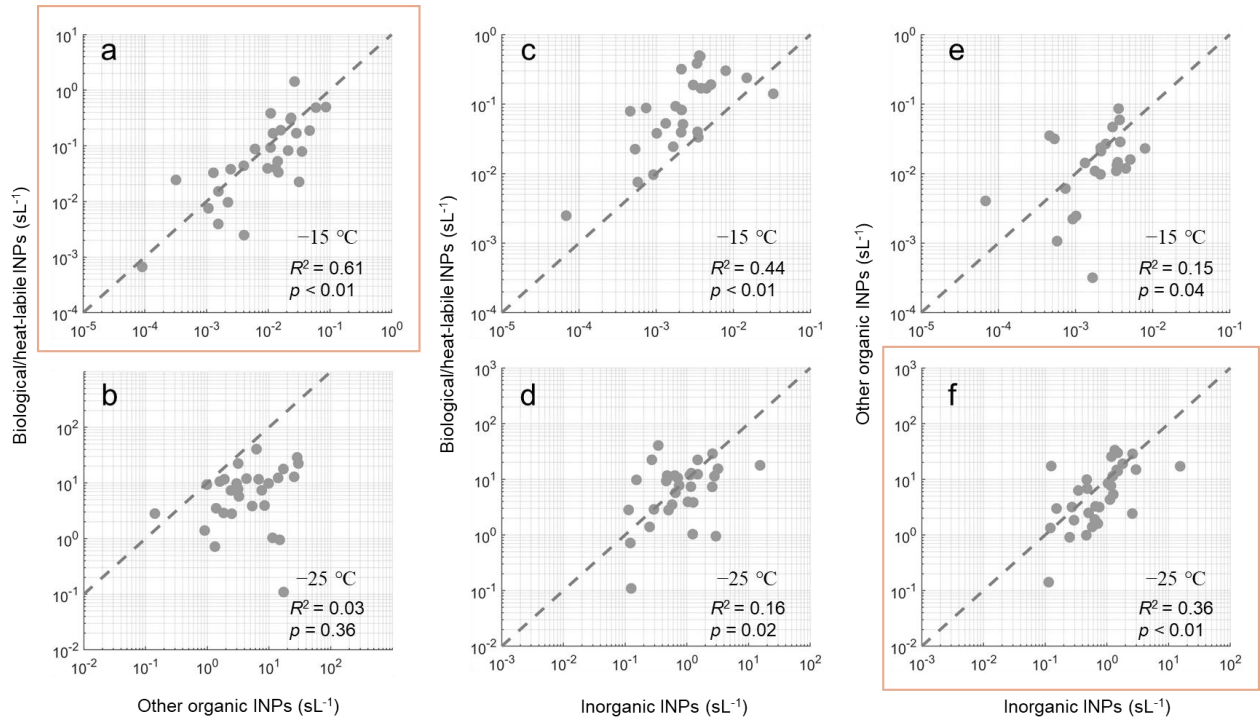
Figure 8. Correlations between concentrations of (a, b) biological/heat-labile INPs and other organic INPs, (c, d) biological/heat-labile INPs and inorganic INPs, and (e, f) other organic INPs and inorganic INPs, active at either −15 °C (upper row) or −25 °C (lower row). Dashed lines indicate a 10:1 relationship for reference, and the orange rectangles highlight the strongest correlations at each temperature.

772
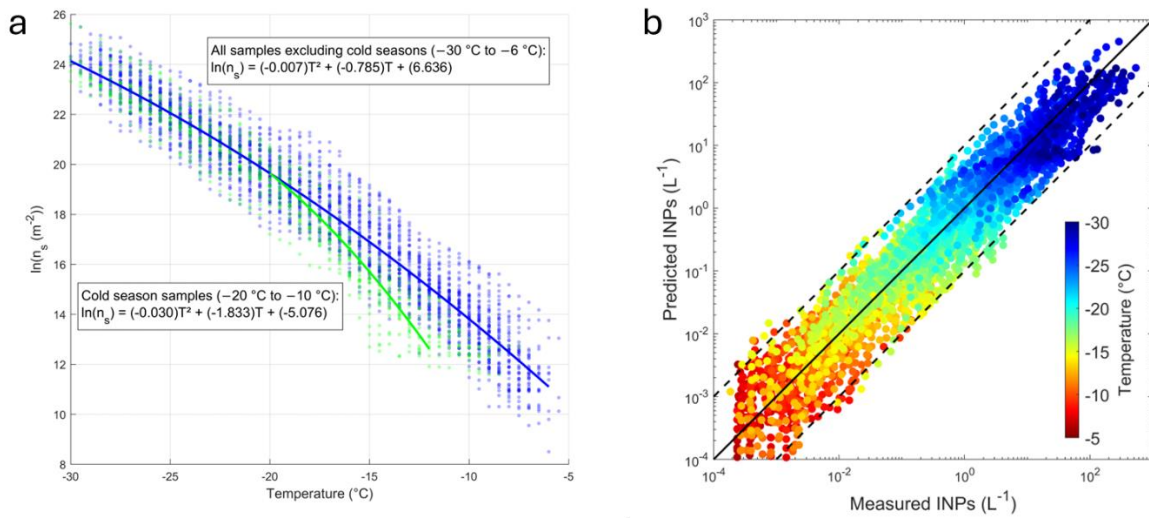
Figure 9. (a) All cold season (December–March) and other seasons (April–November) INP data, expressed as IN active surface site density n_s (based on the surface area of particles larger than 500 nm), with parameterization fits. All samples, excluding those from cold seasons, were used to develop the parameterization equation for temperatures from −30 °C to −6 °C. A separate equation was developed for samples from cold seasons at temperatures from −20 °C to −10 °C. (b) Comparison between predicted INP concentrations based on the parameterization equations and measured surface area concentrations, and measured INP concentrations.

780

781 **Table 1.** Pearson correlation coefficients (R^2) between monthly means of INP concentrations and

782 source factor concentrations.

	Coarse dust	Fine dust	Biomass burning	Sulfate-dominated	Nitrate-dominated	Coarse dust and biomass burning
-10 ℃	0.430*	0.192	0.157	0.070	0.036	0.389*
-15 ℃	0.568*	0.175	0.316*	0.093	0.040	0.590*
-20 ℃	0.579*	0.117	0.484*	0.121	0.040	0.706*
-25 ℃	0.500*	0.100	0.688*	0.147	0.051	0.763*

783 *$p < 0.01$

784

References

Agresti, A. and Coull, B. A.: Approximate is better than "exact" for interval estimation of binomial proportions, Am. Stat., 52, 119-126, 1998.

Ashbaugh, L. L., Malm, W. C., and Sadeh, W. Z.: A residence time probability analysis of sulfur concentrations at Grand Canyon National Park, Atmos. Envrion., 19, 1263-1270, 1985.

Atkinson, J. D., Murray, B. J., Woodhouse, M. T., Whale, T. F., Baustian, K. J., Carslaw, K. S., Dobbie, S., O'Sullivan, D., and Malkin, T. L.: The importance of feldspar for ice nucleation by mineral dust in mixed-phase clouds, Nature, 498, 355-358, https://doi.org/10.1038/nature12278, 2013.

Barry, K. R., Hill, T. C. J., Jentzsch, C., Moffett, B. F., Stratmann, F., and DeMott, P. J.: Pragmatic protocols for working cleanly when measuring ice nucleating particles, Atmos. Res., 250, https://doi.org/10.1016/j.atmosres.2020.105419, 2021a.

Barry, K. R., Hill, T. C. J., Levin, E. J. T., Twohy, C. H., Moore, K. A., Weller, Z. D., Toohey, D. W., Reeves, M., Campos, T., Geiss, R., Schill, G. P., Fischer, E. V., Kreidenweis, S. M., and DeMott, P. J.: Observations of Ice Nucleating Particles in the Free Troposphere From Western US Wildfires, J. Geophys. Res: Atmos., 126, https://doi.org/10.1029/2020jd033752, 2021b.

Beall, C. M., Hill, T. C. J., DeMott, P. J., Köneman, T., Pikridas, M., Drewnick, F., Harder, H., Pöhlker, C., Lelieveld, J., Weber, B., Iakovides, M., Prokes, R., Sciare, J., Andreae, M. O., Stokes, M. D., and Prather, K. A.: Ice-nucleating particles near two major dust source regions, Atmos. Chem. Phys., 22, 12607-12627, https://doi.org/10.5194/acp-22-12607-2022, 2022.

Bigg, E. K.: The supercooling of water, Proceedings of the Physical Society. Section B, 66, 688, 1953.

Bowers, R. M., McCubbin, I. B., Hallar, A. G., and Fierer, N.: Seasonal variability in airborne bacterial communities at a high-elevation site, Atmos. Envrion., 50, 41-49, https://doi.org/10.1016/j.atmosenv.2012.01.005, 2012.

Brown, S. G., Eberly, S., Paatero, P., and Norris, G. A.: Methods for estimating uncertainty in PMF solutions: examples with ambient air and water quality data and guidance on reporting PMF results, Sci. Total Environ., 518-519, 626-635, https://doi.org/10.1016/j.scitotenv.2015.01.022, 2015.

Burrows, S. M., McCluskey, C. S., Cornwell, G., Steinke, I., Zhang, K., Zhao, B., Zawadowicz, M., Raman, A., Kulkarni, G., and China, S.: Ice-nucleating particles that impact clouds and climate: Observational and modeling research needs, Rev. Geophys., 60, e2021RG000745, 2022.

Conen, F. and Yakutin, M. V.: Soils rich in biological ice-nucleating particles abound in ice-nucleating macromolecules likely produced by fungi, Biogeosciences, 15, 4381-4385, https://doi.org/10.5194/bg-15-4381-2018, 2018.

Conen, F., Rodríguez, S., Hülin, C., Henne, S., Herrmann, E., Bukowiecki, N., and Alewell, C.: Atmospheric ice nuclei at the high-altitude observatory Jungfraujoch, Switzerland, Tellus B Chem. Phys. Meteorol., 67, 25014, 2015.

Creamean, J. M., Hill, T. C., Hume, C. C., and Devadoss, T.: Ice Nucleation Spectrometer (INS) Instrument Handbook, Oak Ridge National Laboratory (ORNL), Oak Ridge, TN (United States)

825 Atmospheric Radiation Measurement (ARM) Data Center, https://doi.org/10.2172/1846263,
826 2024.

827 Creamean, J. M., Suski, K. J., Rosenfeld, D., Cazorla, A., DeMott, P. J., Sullivan, R. C., White,
828 A. B., Ralph, F. M., Minnis, P., and Comstock, J. M.: Dust and biological aerosols from the
829 Sahara and Asia influence precipitation in the western US, Science, 339, 1572-1578, 2013.

830 Cornwell, G. C., McCluskey, C. S., Hill, T. C. J., Levin, E. T., Rothfuss, N. E., Tai, S. L., Petters,
831 M. D., DeMott, P. J., Kreidenweis, S., Prather, K. A., and Burrows, S. M.: Bioaerosols are the
832 dominant source of warm-temperature immersion-mode INPs and drive uncertainties in INP
833 predictability, Sci Adv, 9, eadg3715, https://doi.org/10.1126/sciadv.adg3715, 2023.

834 Cornwell, G. C., Steinke, I., Lata, N. N., Zelenyuk, A., Kulkarni, G., Pekour, M., Perkins, R.,
835 Levin, E. J. T., China, S., Demott, P. J., and Burrows, S. M.: Enrichment of Phosphates, Lead,
836 and Mixed Soil-Organic Particles in INPs at the Southern Great Plains Site, J. Geophys. Res:
837 Atmos., 129, https://doi.org/10.1029/2024jd040826, 2024.

838 Cromwell, E., Singh, A., & Kuang, C. Optical Particle Counter (AOSOPC), 2021-10-27 to 2023-
839 06-16, ARM Mobile Facility (GUC), Gunnison, CO; Supplemental Facility 2 (S2). Atmospheric
840 Radiation Measurement (ARM) User Facility. https://doi.org/10.5439/1824224, Data accessed
841 2024-08-01.

842 de Boer, G., Morrison, H., Shupe, M. D., and Hildner, R.: Evidence of liquid dependent ice
843 nucleation in high-latitude stratiform clouds from surface remote sensors, Geophys. Res. Lett.,
844 38, 2011.

845 DeMott, P. J., Sassen, K., Poellot, M. R., Baumgardner, D., Rogers, D. C., Brooks, S. D., Prenni,
846 A. J., and Kreidenweis, S. M.: African dust aerosols as atmospheric ice nuclei, Geophys. Res.
847 Lett., 30, https://doi.org/10.1029/2003gl017410, 2003.

848 DeMott, P. J., Prenni, A. J., Liu, X., Kreidenweis, S. M., Petters, M. D., Twohy, C. H.,
849 Richardson, M. S., Eidhammer, T., and Rogers, D. C.: Predicting global atmospheric ice nuclei
850 distributions and their impacts on climate, Proc. Natl. Acad. Sci. USA, 107, 11217-11222,
851 https://doi.org/10.1073/pnas.0910818107, 2010.

852 DeMott, P. J., Prenni, A. J., McMeeking, G. R., Sullivan, R. C., Petters, M. D., Tobo, Y.,
853 Niemand, M., Möhler, O., Snider, J. R., Wang, Z., and Kreidenweis, S. M.: Integrating laboratory
854 and field data to quantify the immersion freezing ice nucleation activity of mineral dust particles,
855 Atmos. Chem. Phys., 15, 393-409, https://doi.org/10.5194/acp-15-393-2015, 2015.

856 DeMott, P. J., Mirrielees, J. A., Petters, S. S., Cziczo, D. J., Petters, M. D., Bingemer, H. G., Hill,
857 T. C. J., Froyd, K., Garimella, S., Hallar, A. G., Levin, E. J. T., McCubbin, I. B., Perring, A. E.,
858 Rapp, C. N., Schiebel, T., Schrod, J., Suski, K. J., Weber, D., Wolf, M. J., Zawadowicz, M.,
859 Zenker, J., Möhler, O., and Brooks, S. D.: Field intercomparison of ice nucleation measurements:
860 the Fifth International Workshop on Ice Nucleation Phase 3 (FIN-03), Atmos. Meas. Tech., 18,
861 639-672, https://doi.org/10.5194/amt-18-639-2025, 2025.

862 Després, V., Huffman, J. A., Burrows, S. M., Hoose, C., Safatov, A., Buryak, G., Fröhlich-
863 Nowoisky, J., Elbert, W., Andreae, M., Pöschl, U., and Jaenicke, R.: Primary biological aerosol
864 particles in the atmosphere: a review, Tellus B Chem. Phys. Meteorol., 64, 15598,
865 https://doi.org/10.3402/tellusb.v64i0.15598, 2012.

866   Fall, P. L.: Spatial patterns of atmospheric pollen dispersal in the Colorado Rocky Mountains,
867   USA, Review of Palaeobotany and Palynology, 74, 293-313, https://doi.org/10.1016/0034-
868   6667(92)90013-7, 1992.

869   Feldman, D. R., Aiken, A. C., Boos, W. R., Carroll, R. W. H., Chandrasekar, V., Collis, S.,
870   Creamean, J. M., de Boer, G., Deems, J., DeMott, P. J., Fan, J., Flores, A. N., Gochis, D., Grover,
871   M., Hill, T. C. J., Hodshire, A., Hulm, E., Hume, C. C., Jackson, R., Junyent, F., Kennedy, A.,
872   Kumjian, M., Levin, E. J. T., Lundquist, J. D., O'Brien, J., Raleigh, M. S., Reithel, J., Rhoades,
873   A., Rittger, K., Rudisill, W., Sherman, Z., Siirila-Woodburn, E., Skiles, S. M., Smith, J. N.,
874   Sullivan, R. C., Theisen, A., Tuftedal, M., Varble, A. C., Wiedlea, A., Wielandt, S., Williams, K.,
875   and Xu, Z.: The Surface Atmosphere Integrated Field Laboratory (SAIL) Campaign, Bull. Amer.
876   Meteor. Soc., 104, E2192-E2222, https://doi.org/10.1175/bams-d-22-0049.1, 2023.

877   Fröhlich-Nowoisky, J., Kampf, C. J., Weber, B., Huffman, J. A., Pöhlker, C., Andreae, M. O.,
878   Lang-Yona, N., Burrows, S. M., Gunthe, S. S., and Elbert, W.: Bioaerosols in the Earth system:
879   Climate, health, and ecosystem interactions, Atmos. Res., 182, 346-376, 2016.

880   Garcia, E., Hill, T. C., Prenni, A. J., DeMott, P. J., Franc, G. D., and Kreidenweis, S. M.:
881   Biogenic ice nuclei in boundary layer air over two US High Plains agricultural regions, J.
882   Geophys. Res: Atmos., 117, 2012.

883   Ginoux, P., Prospero, J. M., Gill, T. E., Hsu, N. C., and Zhao, M.: Global-scale attribution of
884   anthropogenic and natural dust sources and their emission rates based on MODIS Deep Blue
885   aerosol products, Rev. Geophys., 50, https://doi.org/10.1029/2012rg000388, 2012.

886   Hamzehpour, N., Marcolli, C., Klumpp, K., Thöny, D., and Peter, T.: The Urmia playa as a
887   source of airborne dust and ice-nucleating particles – Part 2: Unraveling the relationship between
888   soil dust composition and ice nucleation activity, Atmos. Chem. Phys., 22, 14931-14956,
889   https://doi.org/10.5194/acp-22-14931-2022, 2022.

890   Hand, J. L. and Kreidenweis, S. M.: A New Method for Retrieving Particle Refractive Index and
891   Effective Density from Aerosol Size Distribution Data, Aerosol Sci. Technol., 36, 1012-1026,
892   https://doi.org/10.1080/02786820290092276, 2002.

893   Hand, J. L., Gill, T. E., and Schichtel, B. A.: Spatial and seasonal variability in fine mineral dust
894   and coarse aerosol mass at remote sites across the United States, J. Geophys. Res: Atmos., 122,
895   3080-3097, https://doi.org/10.1002/2016jd026290, 2017.

896   Hand, J.: IMPROVE Data User Guide 2023 (Version 2), Interagency Monitoring of Protected
897   Visual Environments (IMPROVE) Program, available at:
898   https://vista.cira.colostate.edu/Improve/data-user-guide/, 2023.

899   Harrison, A. D., Lever, K., Sanchez-Marroquin, A., Holden, M. A., Whale, T. F., Tarn, M. D.,
900   McQuaid, J. B., and Murray, B. J.: The ice-nucleating ability of quartz immersed in water and its
901   atmospheric importance compared to K-feldspar, Atmos. Chem. Phys., 19, 11343-11361,
902   https://doi.org/10.5194/acp-19-11343-2019, 2019.

903   Herbert, R. J., Sanchez-Marroquin, A., Grosvenor, D. P., Pringle, K. J., Arnold, S. R., Murray, B.
904   J., and Carslaw, K. S.: Gaps in our understanding of ice-nucleating particle sources exposed by
905   global simulation of the UK Earth System Model, Atmos. Chem. Phys., 25, 291-325, 2025.

Hill, T. C. J., DeMott, P. J., Tobo, Y., Fröhlich-Nowoisky, J., Moffett, B. F., Franc, G. D., and Kreidenweis, S. M.: Sources of organic ice nucleating particles in soils, Atmos. Chem. Phys., 16, 7195-7211, https://doi.org/10.5194/acp-16-7195-2016, 2016.

Hiranuma, N., Augustin-Bauditz, S., Bingemer, H., Budke, C., Curtius, J., Danielczok, A., Diehl, K., Dreischmeier, K., Ebert, M., Frank, F., Hoffmann, N., Kandler, K., Kiselev, A., Koop, T., Leisner, T., Möhler, O., Nillius, B., Peckhaus, A., Rose, D., Weinbruch, S., Wex, H., Boose, Y., DeMott, P. J., Hader, J. D., Hill, T. C. J., Kanji, Z. A., Kulkarni, G., Levin, E. J. T., McCluskey, C. S., Murakami, M., Murray, B. J., Niedermeier, D., Petters, M. D., O'Sullivan, D., Saito, A., Schill, G. P., Tajiri, T., Tolbert, M. A., Welti, A., Whale, T. F., Wright, T. P., and Yamashita, K.: A comprehensive laboratory study on the immersion freezing behavior of illite NX particles: a comparison of 17 ice nucleation measurement techniques, Atmos. Chem. Phys., 15, 2489-2518, https://doi.org/10.5194/acp-15-2489-2015, 2015.

Hoose, C. and Möhler, O.: Heterogeneous ice nucleation on atmospheric aerosols: a review of results from laboratory experiments, Atmos. Chem. Phys., 12, 9817-9854, https://doi.org/10.5194/acp-12-9817-2012, 2012.

Hopke, P. K., Dai, Q., Li, L., and Feng, Y.: Global review of recent source apportionments for airborne particulate matter, Sci. Total Environ., 740, 140091, https://doi.org/10.1016/j.scitotenv.2020.140091, 2020.

Huang, S., Hu, W., Chen, J., Wu, Z. J., Zhang, D. Z., and Fu, P. Q.: Overview of biological ice nucleating particles in the atmosphere, Environ. Int., 146, https://doi.org/10.1016/j.envint.2020.106197, 2021.

Hwang, I. and Hopke, P. K.: Estimation of source apportionment and potential source locations of PM2.5 at a west coastal IMPROVE site, Atmos. Environ., 41, 506-518, https://doi.org/10.1016/j.atmosenv.2006.08.043, 2007.

IPCC, 2022: Climate Change 2022: Impacts, Adaptation, and Vulnerability., Contribution of Working Group II to the Sixth Assessment Report of the Intergovernmental Panel on Climate Change [H.-O. Pörtner, D.C. Roberts, M. Tignor, E.S. Poloczanska, K. Mintenbeck, A. Alegría, M. Craig, S. Langsdorf, S. Löschke, V. Möller, A. Okem, B. Rama (eds.)]. Cambridge University Press. Cambridge University Press, Cambridge, UK and New York, NY, USA, 3056 pp., https://doi.org/10.1017/9781009325844, 2022.

Jahl, L. G., Brubaker, T. A., Polen, M. J., Jahn, L. G., Cain, K. P., Bowers, B. B., Fahy, W. D., Graves, S., and Sullivan, R. C.: Atmospheric aging enhances the ice nucleation ability of biomass-burning aerosol, Sci. Adv., 7, eabd3440, 2021.

Jahn, L. G., Jahl, L. G., Bland, G. D., Bowers, B. B., Monroe, L. W., and Sullivan, R. C.: Metallic and crustal elements in biomass-burning aerosol and ash: Prevalence, significance, and similarity to soil particles, ACS Earth Space Chem., 5, 136-148, 2020.

Jain, P., Sharma, A. R., Acuna, D. C., Abatzoglou, J. T., and Flannigan, M.: Record-breaking fire weather in North America in 2021 was initiated by the Pacific northwest heat dome, Commun. Earth Environ., 5, 202, 2024.

Kanji, Z. A., Ladino, L. A., Wex, H., Boose, Y., Burkert-Kohn, M., Cziczo, D. J., and Krämer, M.: Overview of Ice Nucleating Particles, Meteor. Monogr., 58, 1.1-1.33, https://doi.org/10.1175/amsmonographs-d-16-0006.1, 2017.

948 Kiselev, A., Bachmann, F., Pedevilla, P., Cox, S. J., Michaelides, A., Gerthsen, D., and Leisner,
949 T.: Active sites in heterogeneous ice nucleation-the example of K-rich feldspars, Science, 355,
950 367-371, https://doi.org/10.1126/science.aai8034, 2017.

951 Knippertz, P. and Stuut, J.-B. W.: Mineral dust, Mineral dust—A key player in the Earth system,
952 121-147, Springer, 2014.

953 Kobziar, L. N., Lampman, P., Tohidi, A., Kochanski, A. K., Cervantes, A., Hudak, A. T.,
954 McCarley, R., Gullett, B., Aurell, J., and Moore, R.: Bacterial emission factors: a foundation for
955 the terrestrial-atmospheric modeling of bacteria aerosolized by wildland fires, Environ. Sci.
956 Technol., 58, 2413-2422, 2024.

957 Koehler, K. A., Kreidenweis, S. M., DeMott, P. J., Prenni, A. J., and Petters, M. D.: Potential
958 impact of Owens (dry) Lake dust on warm and cold cloud formation, J. Geophys. Res: Atmos.,
959 112, 2007.

960 Kotchenruther, R. A.: Source apportionment of $PM_{2.5}$ at IMPROVE monitoring sites within and
961 outside of marine vessel fuel sulfur emissions control areas, J Air Waste Manag Assoc, 71, 1114-
962 1126, https://doi.org/10.1080/10962247.2021.1917463, 2021.

963 Kuang, C., Singh, A., Howie, J., Salwen, C., & Hayes, C. Scanning mobility particle sizer
964 (AOSSMPS), 2021-10-27 to 2023-06-16, ARM Mobile Facility (GUC), Gunnison, CO;
965 Supplemental Facility 2 (S2). Atmospheric Radiation Measurement (ARM) User Facility.
966 https://doi.org/10.5439/1476898, Data accessed 2024-08-01.

967 Lacher, L., Steinbacher, M., Bukowiecki, N., Herrmann, E., Zipori, A., and Kanji, Z. A.: Impact
968 of Air Mass Conditions and Aerosol Properties on Ice Nucleating Particle Concentrations at the
969 High Altitude Research Station Jungfraujoch, Atmosphere, 9,
970 https://doi.org/10.3390/atmos9090363, 2018.

971 Liu, W. and Hopke, P. K.: Origins of fine aerosol mass in the western United States using positive
972 matrix factorization, J. Geophys. Res: Atmos., 108, https://doi.org/10.1029/2003jd003678, 2003.

973 Lohmann, U. and Feichter, J.: Global indirect aerosol effects: a review, Atmos. Chem. Phys., 5,
974 715-737, https://doi.org/10.5194/acp-5-715-2005, 2005.

975 Lynn, B., Khain, A., Rosenfeld, D., and Woodley, W. L.: Effects of aerosols on precipitation from
976 orographic clouds, J. Geophys. Res: Atmos., 112, 2007.

977 Malm, W. C., Sisler, J. F., Huffman, D., Eldred, R. A., and Cahill, T. A.: Spatial and seasonal
978 trends in particle concentration and optical extinction in the United States, J. Geophys. Res:
979 Atmos., 99, 1347-1370, 1994.

980 Marinescu, P. J., Levin, E. J., Collins, D., Kreidenweis, S. M., and van den Heever, S. C.:
981 Quantifying aerosol size distributions and their temporal variability in the Southern Great Plains,
982 USA, Atmos. Chem. Phys., 19, 11985-12006, 2019.

983 McCluskey, C. S., DeMott, P. J., Prenni, A. J., Levin, E. J. T., McMeeking, G. R., Sullivan, A. P.,
984 Hill, T. C. J., Nakao, S., Carrico, C. M., and Kreidenweis, S. M.: Characteristics of atmospheric
985 ice nucleating particles associated with biomass burning in the US: Prescribed burns and
986 wildfires, J. Geophys. Res: Atmos., 119, 10458-10470, https://doi.org/10.1002/2014jd021980,
987 2014.

McCluskey, C. S., Ovadnevaite, J., Rinaldi, M., Atkinson, J., Belosi, F., Ceburnis, D., Marullo, S., Hill, T. C. J., Lohmann, U., Kanji, Z. A., O'Dowd, C., Kreidenweis, S. M., and DeMott, P. J.: Marine and Terrestrial Organic Ice-Nucleating Particles in Pristine Marine to Continentally Influenced Northeast Atlantic Air Masses, J. Geophys. Res: Atmos., 123, 6196-6212, https://doi.org/10.1029/2017jd028033, 2018a.

McCluskey, C. S., Hill, T. C. J., Malfatti, F., Sultana, C. M., Lee, C., Santander, M. V., Beall, C. M., Moore, K. A., Cornwell, G. C., Collins, D. B., Prather, K. A., Jayarathne, T., Stone, E. A., Azam, F., Kreidenweis, S. M., and DeMott, P. J.: A Dynamic Link between Ice Nucleating Particles Released in Nascent Sea Spray Aerosol and Oceanic Biological Activity during Two Mesocosm Experiments, J. Atmos. Sci., 74, 151-166, https://doi.org/10.1175/Jas-D-16-0087.1, 2017.

McCluskey, C. S., Hill, T. C. J., Humphries, R. S., Rauker, A. M., Moreau, S., Strutton, P. G., Chambers, S. D., Williams, A. G., McRobert, I., Ward, J., Keywood, M. D., Harnwell, J., Ponsonby, W., Loh, Z. M., Krummel, P. B., Protat, A., Kreidenweis, S. M., and DeMott, P. J.: Observations of Ice Nucleating Particles Over Southern Ocean Waters, Geophys. Res. Lett., 45, https://doi.org/10.1029/2018gl079981, 2018b.

Meng, X., Yu, Y., and Ginoux, P.: Rise in dust emissions from burned landscapes primarily driven by small fires, Nat. Geosci., 18, 586-592, https://doi.org/10.1038/s41561-025-01730-3, 2025.

Meyers, M. P., DeMott, P. J., and Cotton, W. R.: New primary ice-nucleation parameterizations in an explicit cloud model, J. Appl. Meteor. Climatol., 31, 708-721, 1992.

Miltenberger, A. K., Field, P. R., Hill, A. A., Rosenberg, P., Shipway, B. J., Wilkinson, J. M., Scovell, R., and Blyth, A. M.: Aerosol–cloud interactions in mixed-phase convective clouds–Part 1: Aerosol perturbations, Atmos. Chem. Phys., 18, 3119-3145, 2018.

Mignani, C., Hill, T. C. J., Nieto-Caballero, M., Barry, K. R., Bryan, N. C., Marinescu, P. J., Dolan, B., Sullivan, A. P., Hernandez, M., Bosco-Lauth, A., van den Heever, S. C., Stone, E. A., Grant, L. D., Perkins, R. J., DeMott, P. J., and Kreidenweis, S. M.: Ice-Nucleating Particles Are Emitted by Raindrop Impact, J. Geophys. Res: Atmos., 130, https://doi.org/10.1029/2024jd042584, 2025.

Murray, B. J., O'Sullivan, D., Atkinson, J. D., and Webb, M. E.: Ice nucleation by particles immersed in supercooled cloud droplets, Chem Soc Rev, 41, 6519-6554, https://doi.org/10.1039/c2cs35200a, 2012.

Niemand, M., Möhler, O., Vogel, B., Vogel, H., Hoose, C., Connolly, P., Klein, H., Bingemer, H., DeMott, P., Skrotzki, J., and Leisner, T.: A Particle-Surface-Area-Based Parameterization of Immersion Freezing on Desert Dust Particles, J. Atmos. Sci., 69, 3077-3092, https://doi.org/10.1175/Jas-D-11-0249.1, 2012.

Norris, G., Duvall, R., Brown, S., and Bai, S.: EPA positive matrix factorization (PMF) 5.0 fundamentals and user guide, US Environmental Protection Agency, Washington, DC, www2. epa. gov/sites/production/files/2015-02/documents/pmf_5. 0_user_guide. pdf, 2014.

O'Sullivan, D., Murray, B. J., Ross, J. F., and Webb, M. E.: The adsorption of fungal ice-nucleating proteins on mineral dusts: a terrestrial reservoir of atmospheric ice-nucleating particles, Atmos. Chem. Phys., 16, 7879-7887, https://doi.org/10.5194/acp-16-7879-2016, 2016.

O'Sullivan, D., Murray, B. J., Malkin, T. L., Whale, T. F., Umo, N. S., Atkinson, J. D., Price, H. C., Baustian, K. J., Browse, J., and Webb, M. E.: Ice nucleation by fertile soil dusts: relative importance of mineral and biogenic components, Atmos. Chem. Phys., 14, 1853-1867, https://doi.org/10.5194/acp-14-1853-2014, 2014.

Pereira, D. L., Gavilán, I., Letechipía, C., Raga, G. B., Puig, T. P., Mugica-Álvarez, V., Alvarez-Ospina, H., Rosas, I., Martinez, L., Salinas, E., Quintana, E. T., Rosas, D., and Ladino, L. A.: Mexican agricultural soil dust as a source of ice nucleating particles, Atmos. Chem. Phys., 22, 6435-6447, https://doi.org/10.5194/acp-22-6435-2022, 2022.

Pratt, K. A., DeMott, P. J., French, J. R., Wang, Z., Westphal, D. L., Heymsfield, A. J., Twohy, C. H., Prenni, A. J., and Prather, K. A.: In situ detection of biological particles in cloud ice-crystals, Nat. Geosci., 2, 398-401, https://doi.org/10.1038/ngeo521, 2009.

Pratt, K. A., Twohy, C. H., Murphy, S. M., Moffet, R. C., Heymsfield, A. J., Gaston, C. J., DeMott, P. J., Field, P. R., Henn, T. R., Rogers, D. C., Gilles, M. K., Seinfeld, J. H., and Prather, K. A.: Observation of playa salts as nuclei in orographic wave clouds, J. Geophys. Res: Atmos., 115, https://doi.org/10.1029/2009jd013606, 2010.

Prenni, A. J., DeMott, P. J., Sullivan, A. P., Sullivan, R. C., Kreidenweis, S. M., and Rogers, D. C.: Biomass burning as a potential source for atmospheric ice nuclei: Western wildfires and prescribed burns, Geophys. Res. Lett., 39, https://doi.org/10.1029/2012gl051915, 2012.

Prenni, A. J., Tobo, Y., Garcia, E., DeMott, P. J., Huffman, J. A., McCluskey, C. S., Kreidenweis, S. M., Prenni, J. E., Pöhlker, C., and Pöschl, U.: The impact of rain on ice nuclei populations at a forested site in Colorado, Geophys. Res. Lett., 40, 227-231, https://doi.org/10.1029/2012gl053953, 2013.

Reicher, N., Budke, C., Eickhoff, L., Raveh-Rubin, S., Kaplan-Ashiri, I., Koop, T., and Rudich, Y.: Size-dependent ice nucleation by airborne particles during dust events in the eastern Mediterranean, Atmos. Chem. Phys., 19, 11143-11158, 2019.

Rolph, G., Stein, A., and Stunder, B.: Real-time environmental applications and display system: READY, Environ. Model. Softw., 95, 210-228, 2017.

Sanchez-Marroquin, A., West, J. S., Burke, I. T., McQuaid, J. B., and Murray, B. J.: Mineral and biological ice-nucleating particles above the South East of the British Isles, Environ Sci Atmos, 1, 176-191, https://doi.org/10.1039/d1ea00003a, 2021.

Schill, G. P., DeMott, P. J., Emerson, E. W., Rauker, A. M. C., Kodros, J. K., Suski, K. J., Hill, T. C. J., Levin, E. J. T., Pierce, J. R., Farmer, D. K., and Kreidenweis, S. M.: The contribution of black carbon to global ice nucleating particle concentrations relevant to mixed-phase clouds, Proc. Natl. Acad. Sci. USA, 117, 22705-22711, https://doi.org/10.1073/pnas.2001674117, 2020.

Schnell, R. C. and Vali, G.: Looking Back: An Account of How Ice Nucleation by Bacteria Was Discovered (1963 to about Mid-1980s). Part II: Broadening the Scope, Bull. Amer. Meteor. Soc., 105, E1004-E1014, https://doi.org/10.1175/bams-d-23-0115.1, 2024.

Seinfeld, J. H. and Pandis, S. N.: Atmospheric chemistry and physics: from air pollution to climate change, 3rd edn., Wiley, Hoboken, NJ, 2016.

Seinfeld, J. H., Bretherton, C., Carslaw, K. S., Coe, H., DeMott, P. J., Dunlea, E. J., Feingold, G., Ghan, S., Guenther, A. B., Kahn, R., Kraucunas, I., Kreidenweis, S. M., Molina, M. J., Nenes,

A., Penner, J. E., Prather, K. A., Ramanathan, V., Ramaswamy, V., Rasch, P. J., Ravishankara, A. R., Rosenfeld, D., Stephens, G., and Wood, R.: Improving our fundamental understanding of the role of aerosol-cloud interactions in the climate system, Proc. Natl. Acad. Sci. USA, 113, 5781-5790, https://doi.org/10.1073/pnas.1514043113, 2016.

Shawon, A. S. M., Benedict, K. B., Gutierrez, A., and Aiken, A. C.: Diurnal Trends and Meteorological Factors Influencing the Variability of Fluorescent Bioaerosol in Mt. Crested Butte, Colorado During SAIL, J. Geophys. Res: Atmos., 130, https://doi.org/10.1029/2024jd041186, 2025.

Shi, Y., Creamean, J., Hill, T., Hume, C., & Vazquez, M. Ice Nucleation Spectrometer for INP measurement (INP), 2021-09-09 to 2023-06-12, ARM Mobile Facility (GUC), Gunnison, CO; Supplemental Facility 2 (S2). Atmospheric Radiation Measurement (ARM) User Facility. https://doi.org/10.5439/1770816, Data accessed 2025-05-01.

Shi, Y. and Liu, X.: Dust radiative effects on climate by glaciating mixed-phase clouds, Geophys. Res. Lett., 46, 6128-6137, 2019.

Stein, A. F., Draxler, R. R., Rolph, G. D., Stunder, B. J., Cohen, M. D., and Ngan, F.: NOAA's HYSPLIT atmospheric transport and dispersion modeling system, Bull. Amer. Meteor. Soc., 96, 2059-2077, 2015.

Steinke, I., Funk, R., Busse, J., Iturri, A., Kirchen, S., Leue, M., Möhler, O., Schwartz, T., Schnaiter, M., Sierau, B., Toprak, E., Ullrich, R., Ulrich, A., Hoose, C., and Leisner, T.: Ice nucleation activity of agricultural soil dust aerosols from Mongolia, Argentina, and Germany, J. Geophys. Res: Atmos., 121, https://doi.org/10.1002/2016jd025160, 2016.

Storelvmo, T., Hoose, C., and Eriksson, P.: Global modeling of mixed-phase clouds: The albedo and lifetime effects of aerosols, J. Geophys. Res: Atmos., 116, 2011.

Sun, Y., Zhu, Y., Qi, Y., Chen, L., Mu, J., Shan, Y., Yang, Y., Nie, Y., Liu, P., Cui, C., Zhang, J., Liu, M., Zhang, L., Wang, Y., Wang, X., Tang, M., Wang, W., and Xue, L.: Measurement report: Atmospheric ice nuclei in the Changbai Mountains (2623 m a.s.l.) in northeastern Asia, Atmos. Chem. Phys., 24, 3241-3256, https://doi.org/10.5194/acp-24-3241-2024, 2024.

Suski, K. J., Hill, T. C., Levin, E. J., Miller, A., DeMott, P. J., and Kreidenweis, S. M.: Agricultural harvesting emissions of ice-nucleating particles, Atmos. Chem. Phys., 18, 13755-13771, 2018.

Testa, B., Hill, T. C. J., Marsden, N. A., Barry, K. R., Hume, C. C., Bian, Q., Uetake, J., Hare, H., Perkins, R. J., Möhler, O., Kreidenweis, S. M., and DeMott, P. J.: Ice Nucleating Particle Connections to Regional Argentinian Land Surface Emissions and Weather During the Cloud, Aerosol, and Complex Terrain Interactions Experiment, J. Geophys. Res: Atmos., 126, https://doi.org/10.1029/2021jd035186, 2021.

Tobo, Y., DeMott, P. J., Hill, T. C. J., Prenni, A. J., Swoboda-Colberg, N. G., Franc, G. D., and Kreidenweis, S. M.: Organic matter matters for ice nuclei of agricultural soil origin, Atmos. Chem. Phys., 14, 8521-8531, https://doi.org/10.5194/acp-14-8521-2014, 2014.

Tobo, Y., Prenni, A. J., DeMott, P. J., Huffman, J. A., McCluskey, C. S., Tian, G., Pöhlker, C., Pöschl, U., and Kreidenweis, S. M.: Biological aerosol particles as a key determinant of ice nuclei populations in a forest ecosystem, J. Geophys. Res: Atmos., 118, https://doi.org/10.1002/jgrd.50801, 2013.

1113 Umo, N. S., Murray, B. J., Baeza-Romero, M. T., Jones, J. M., Lea-Langton, A. R., Malkin, T. L.,
1114 O'Sullivan, D., Neve, L., Plane, J. M. C., and Williams, A.: Ice nucleation by combustion ash
1115 particles at conditions relevant to mixed-phase clouds, Atmos. Chem. Phys., 15, 5195-5210,
1116 https://doi.org/10.5194/acp-15-5195-2015, 2015.

1117 Vali, G.: Quantitative evaluation of experimental results on the heterogeneous freezing
1118 nucleation of supercooled liquids, J. Atmos. Sci., 28, 402-409, 1971.

1119 Vali, G. and Schnell, R. C.: Looking Back: An Account of How Ice Nucleation by Bacteria Was
1120 Discovered (1963 to about Mid-1980s). Part I: The Basics, Bull. Amer. Meteor. Soc., 105, E778-
1121 E788, https://doi.org/10.1175/bams-d-23-0114.1, 2024.

1122 Viviroli, D., Dürr, H. H., Messerli, B., Meybeck, M., and Weingartner, R.: Mountains of the
1123 world, water towers for humanity: Typology, mapping, and global significance, Water Resour.
1124 Res., 43, 2007.

1125 Wagner, R., Jähn, M., and Schepanski, K.: Wildfires as a source of airborne mineral dust—
1126 revisiting a conceptual model using large-eddy simulation (LES), Atmos. Chem. Phys., 18,
1127 11863-11884, 2018.

1128 Wilson, T. W., Ladino, L. A., Alpert, P. A., Breckels, M. N., Brooks, I. M., Browse, J., Burrows,
1129 S. M., Carslaw, K. S., Huffman, J. A., Judd, C., Kilthau, W. P., Mason, R. H., McFiggans, G.,
1130 Miller, L. A., Najera, J. J., Polishchuk, E., Rae, S., Schiller, C. L., Si, M., Temprado, J. V., Whale,
1131 T. F., Wong, J. P., Wurl, O., Yakobi-Hancock, J. D., Abbatt, J. P., Aller, J. Y., Bertram, A. K.,
1132 Knopf, D. A., and Murray, B. J.: A marine biogenic source of atmospheric ice-nucleating
1133 particles, Nature, 525, 234-238, https://doi.org/10.1038/nature14986, 2015.

1134 Zhao, X., Jiang, K., Ou'yang, S., Li, Y., Wang, Y., Wang, J., Zhao, N., and Shen, G.: Global
1135 Biomass Burning Emission Contributions to Ice Nucleating Particles, Geophys. Res. Lett., 51,
1136 https://doi.org/10.1029/2024gl111881, 2024.

1137 Ruichen Zhou, Russell Perkins, Sonia Kreidenweis. Source apportionment of aerosols at the White
1138 River IMPROVE site near the SAIL site. ARM Data Collection, Oak Ridge National Laboratory,
1139 U.S. Department of Energy, Oak Ridge, Tennessee, USA. Dataset accessed on 2025.
1140 https://doi.org/10.5439/2573028, 2025a.

1141 Ruichen Zhou, Russell Perkins, Sonia Kreidenweis, Kelton Ayars. Back trajectories during SAIL.
1142 ARM Data Collection, Oak Ridge National Laboratory, U.S. Department of Energy, Oak Ridge,
1143 Tennessee, USA. Dataset accessed on 2025. https://doi.org/10.5439/2574969, 2025a.

1144 Ruichen Zhou, Russell Perkins, Sonia Kreidenweis. Merged aerosol size distribution from SMPS
1145 and OPC for SAIL. ARM Data Collection, Oak Ridge National Laboratory, U.S. Department of
1146 Energy, Oak Ridge, Tennessee, USA. Dataset accessed on 2025.
1147 https://doi.org/10.5439/2572899, 2025a.

1148